Electronic Supplementary Material (ESI) for Physical Chemistry Chemical Physics.
This journal is © the Owner Societies 2016

RIDME Spectroscopy on High-Spin Mn^{2+} Centers

Supporting Information

D. Akhmetzyanov,‡[a] H. Y. V. Ching,‡[b] V. Denysenkov,[a] P. Demay-Drouhard,[c,d] H. C. Bertrand,[c,d] L. C. Tabares,[b] C. Policar,[c,d] T. F Prisner*[a] and S. Un*[b]

[a] Goethe-University Frankfurt am Main, Institute of Physical and Theoretical Chemistry and Center for Biomolecular Magnetic Resonance, Max von Laue Str. 7, 60438 Frankfurt am Main, Germany

[b] Institute for Integrative Biology of the Cell (I2BC), Department of Biochemistry, Biophysics and Structural Biology, Université Paris-Saclay, CEA, CNRS UMR 9198, Gif-sur-Yvette, F-91198, France.

[c] Département de Chimie, Ecole Normale Supérieure, PSL Research University, UPMC Univ Paris 06, CNRS, Laboratoire des Biomolécules (LBM), 24 rue Lhomond, 75005 Paris, France.

[d] Sorbonne Universités, UPMC Univ Paris 06, Ecole Normale Supérieure, CNRS, Laboratoire des Biomolécules (LBM), 24 rue Lhomond, 75005 Paris, France.

‡ Authors contributed equally to the work
* Corresponding authors

Table of contents

1. Chemical structure of mono-MnDOTA complex

Chemical structure of mono-MnDOTA (compound **2**) is depicted in Figure S1.

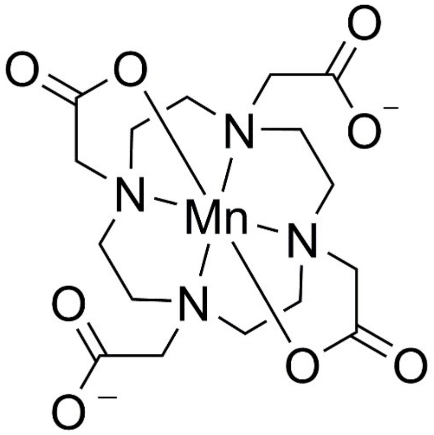

Figure S1. Chemical structure of compound **2**

2. W-band RIDME on compound **1** in deuterated solvent with different pulse lengths

W-band RIDME time traces on compound **1** in a deuterated solvent (D_2O:glycerol-d_8, 4:1, v:v, with 100 mM HEPES at pD 8) obtained with different pulses lengths 10/20 ns (hard pulses) and 40/80 ns (soft pulses) with analysis based on Tikhonov regularization in DeerAnalysis toolbox[1] are shown in Figure S2. The intensity of the second dipolar-coupling frequency harmonic, seen in the time traces and the corresponding distance distribution, is reduced for the case of long pulses. This can be attributed to significantly reduced excitation bandwidth of 80 ns π pulse with respect to 20 ns π pulse and as a result the multiple dipolar coupling frequency components are artificially supressed in the corresponding RIDME time trace.

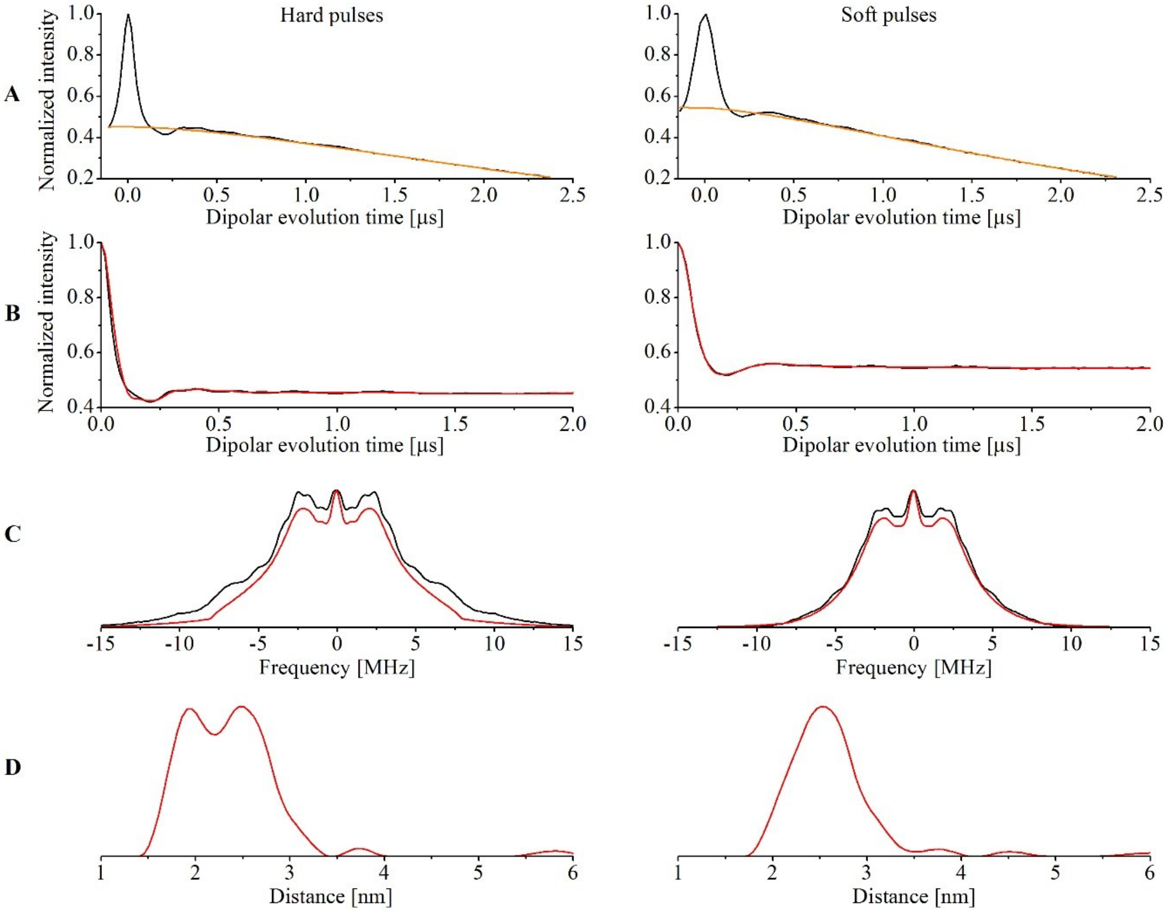

Figure S2. A. Experimental W-band RIDME time trace obtained on compound **1** at 25 K (black lines) in a deuterated solvent, with corresponding stretched-exponential background function (orange lines). Left side. RIDME time traces obtained with hard pulses (π-pulse length of 20 ns). Right side. RIDME time traces obtained with soft pulses (π-pulse length of 80 ns). The spectral position, where the time traces were obtained, corresponded to highest-field hyperfine coupling component (See Figure 3). RIDME time traces were obtained with mixing time of 80 μs.

B. Background-divided RIDME time traces (black lines) with corresponding fits based on Tikhonov regularization analysis (red lines) obtained in DeerAnalysis with a regularization parameter of 10.

C. Fourier transform of background-divided RIDME time traces (black lines) and of the Tikhonov regularization fits (red lines).

D. Distance distributions obtained with Tikhonov regularization analysis.

3. W-band RIDME on compound **1** in protonated solvent with different pulse lengths

W-band RIDME time traces on compound **1** in a protonated solvent (H_2O:glycerol, 4:1, v:v, with 100 mM HEPES at pH 8) obtained with different pulses lengths 10/20 ns (hard pulses) and 40/80 ns (soft pulses) with analysis based on Tikhonov regularization in DeerAnalysis toolbox are depicted in Figure S3. The background functions of these RIDME time traces decay significantly faster than the corresponding background functions of RIDME time traces obtained with a sample in a deuterated solvent (Figure S2). This effect is attributed to proton nuclear spin diffusion that leads to fast decay of the refocused virtual echo. This effect significantly complicates the background-correction procedure and further analysis of the dipolar evolution functions. Therefore, subsequent RIDME experiments were performed with a sample dissolved in a deuterated solvent.

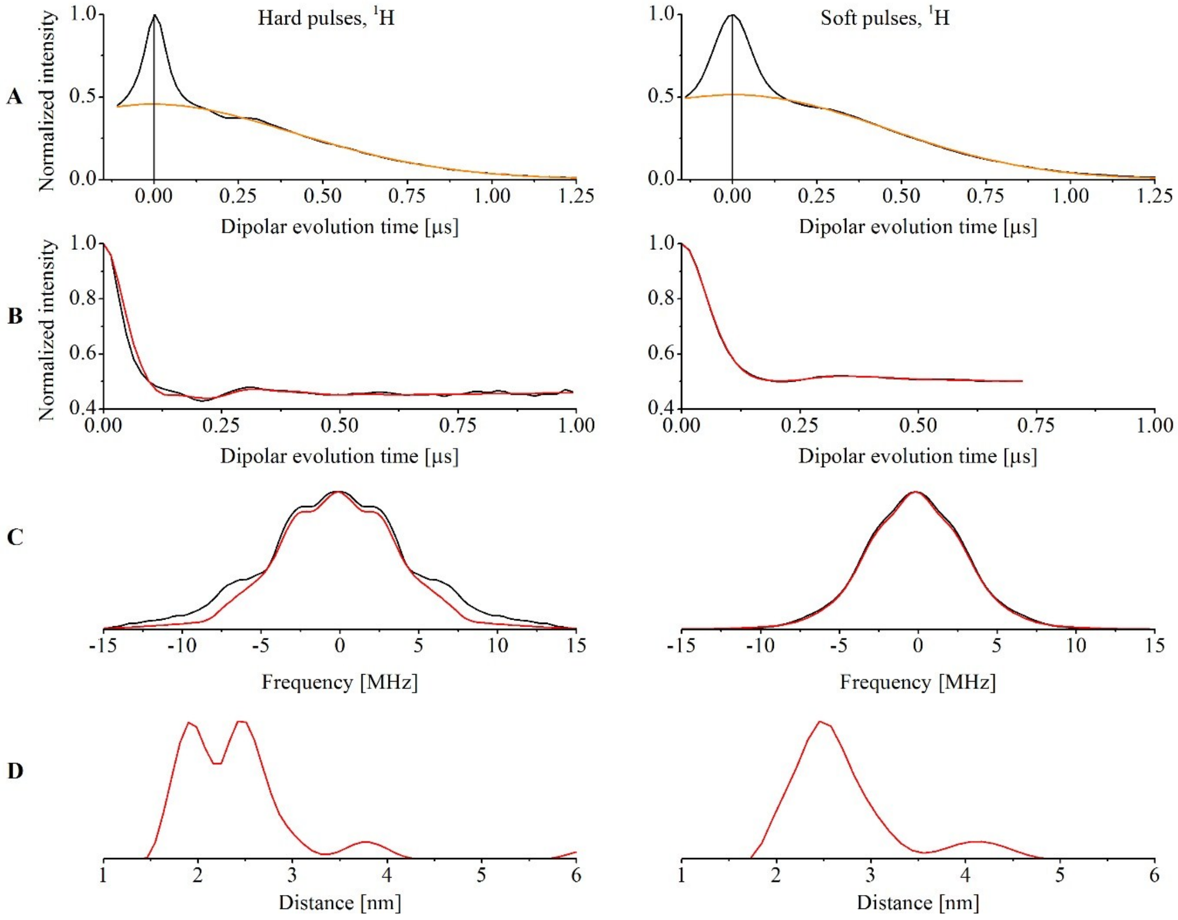

Figure S3. A. Experimental W-band RIDME time trace obtained on compound **1** at 25 K (black lines) in protonated solvent, with corresponding stretched-exponential background function (orange lines). Left side. RIDME time traces obtained with hard pulses (π-pulse length of 20 ns). Right side. RIDME time traces obtained with soft pulses (π-pulse length of 80 ns). The spectral position, where the time traces were obtained corresponded to the highest-field hyperfine coupling component (See Figure 3). RIDME time traces were obtained with mixing time of 80 μs.

B. Background-divided RIDME time traces (black lines) with corresponding fits based on Tikhonov regularization analysis (red lines) obtained in DeerAnalysis with a regularization parameter of 10.

C. Fourier transform of background-divided RIDME time traces (black lines) and of the Tikhonov regularization fits (red lines).

D. Distance distributions obtained with Tikhonov regularization analysis.

4. W-band RIDME on compound **1** in protonated solvent obtained at different spectral positions

W-band RIDME time traces on compound **1** in protonated solvent were obtained at three different position in the EPR spectrum. The first position was chosen to be on resonance with the highest field hyperfine line (the data are shown in Figure S3 - left). The second resonance field position was set 100 G larger than the position of the highest field hyperfine line and the third position was set in the middle between the 3rd and the 4th hyperfine lines. The background-divided RIDME time traces, corresponding Fourier transforms and distance distributions, obtained by Tikhonov regularization with conventional kernel function, are shown in Figure S4.

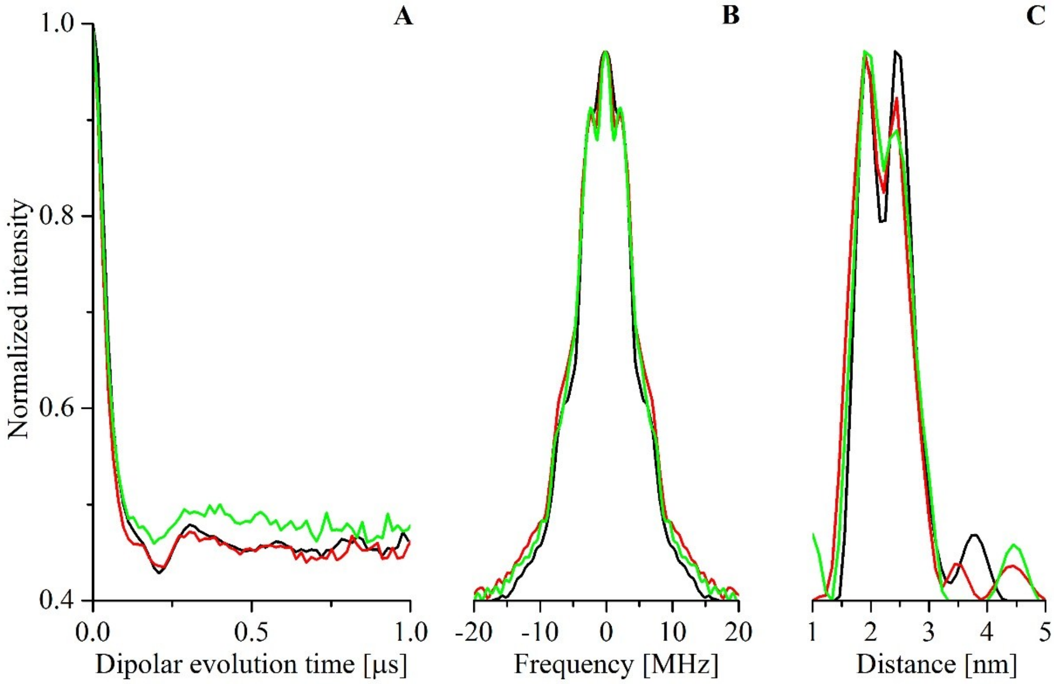

Figure S4. A. Background-divided W-band RIDME time trace obtained on compound **1** in protonated solvent at 25 K (hard pulses). The spectral positions, where the time traces were obtained, corresponded to the highest hyperfine coupling component (black), 100 G larger than the highest hyperfine coupling component (red) and the middle between 3rd and 4th hyperfine components (green). **B.** Corresponding Fourier transforms. **C.** Corresponding distance distributions, obtained by Tikhonov regularization with conventional kernel function in DeerAnalysis toolbox with a regularization parameter of 10.

Insignificant changes were observed in the RIDME time traces (and corresponding Fourier transforms and distance distributions) upon changing the resonance position. As the spectral position, corresponding to the highest hyperfine line, is the most sensitive, it was used for further RIDME studies.

5. RIDME on mono-MnDOTA complex in deuterated and protonated solvents obtained at W-band frequencies

W-band RIDME experimental time traces on mono-MnDOTA (compound **2**) obtained with hard and soft pulses are depicted in Figure S5. The measurements were performed with a sample in deuterated (D_2O:glycerol-d_8, 4:1, v:v, with 100 mM HEPES at pD 8) and protonated solvents (H_2O:glycerol, 4:1, v:v, with 100 mM HEPES at pH 8).

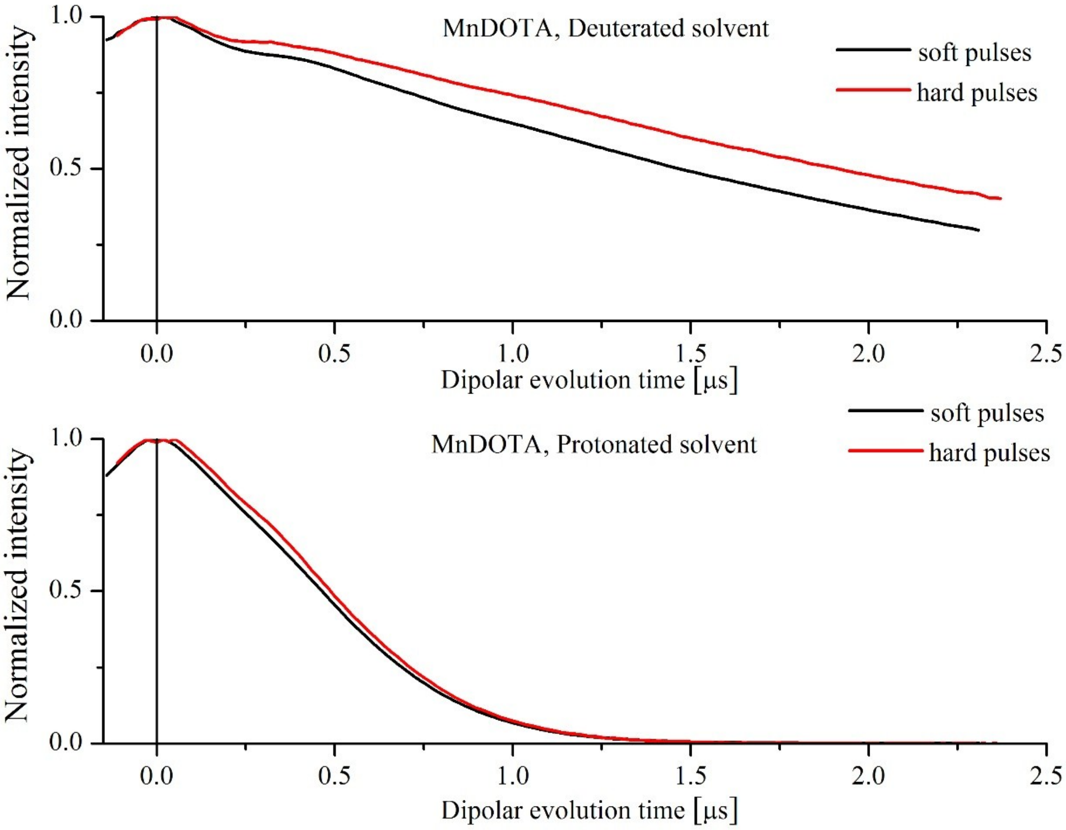

Figure S5. Top. RIDME experimental time traces on compound **2** in a deuterated solvent. The time traces are obtained with soft (black) and hard (red) pulses. Bottom. RIDME time traces on compound **2** in a protonated solvent. The time traces are obtained with soft (black) and hard (red) pulses. The mixing time for all experiments was 80 μs.

RIDME experimental time traces on mono-MnDOTA (compound **2**) with corresponding stretched exponential background function as well as background-divided time traces with corresponding Fourier transforms are depicted in Figure S6. The RIDME time traces, obtained with compound **2** in deuterated solvent, reveal an oscillation with a frequency of about 1.7 MHz. This value corresponded to isotropic hyperfine coupling of Mn^{2+} with 4 equivalent nitrogen nuclei belonging to the DOTA ring. This coupling has been determined by ELDOR detected NMR experiment on similar MnDOTA complex in another study.[2] It is worth noting that the frequency of the oscillation, revealed by RIDME experiment, corresponds purely to the ^{14}N hyperfine coupling, but not the combination of the hyperfine coupling frequency with the ^{14}N Larmor frequency (ν_L of about 10 MHz at W-band frequencies), as would be expected for coherent ESEEM effect. Thus, this oscillation, possibly appears due to incoherent ESEEM effect. This effect has been studied in detail on nitroxide radical in the temperature range of 130 K - 240 K at X-band frequencies and appeared due to the relaxation of protons from the methyl group.[3] Thus, upon fast reorientation of the methyl groups, the proton hyperfine coupling fluctuates, which causes nuclear relaxation.[3] In our case, the effect is assumed to appear due to nitrogen nuclei relaxation. The longitudinal relaxation rate of the ^{14}N is enhanced due to the coupling to fast relaxing Mn^{2+} ions. The fact that the modulation depth of nuclear oscillations of about 3-4 % is an order of magnitude lower than the modulation depth of dipolar oscillation, indicates that ^{14}N longitudinal relaxation is significantly longer than that of electron spin (1 to 2 orders of magnitude). Note also that the presence of four equivalent ^{14}N nuclei significantly increases the probability of one of the ^{14}N nuclei undergoing an arbitrary spin flip.

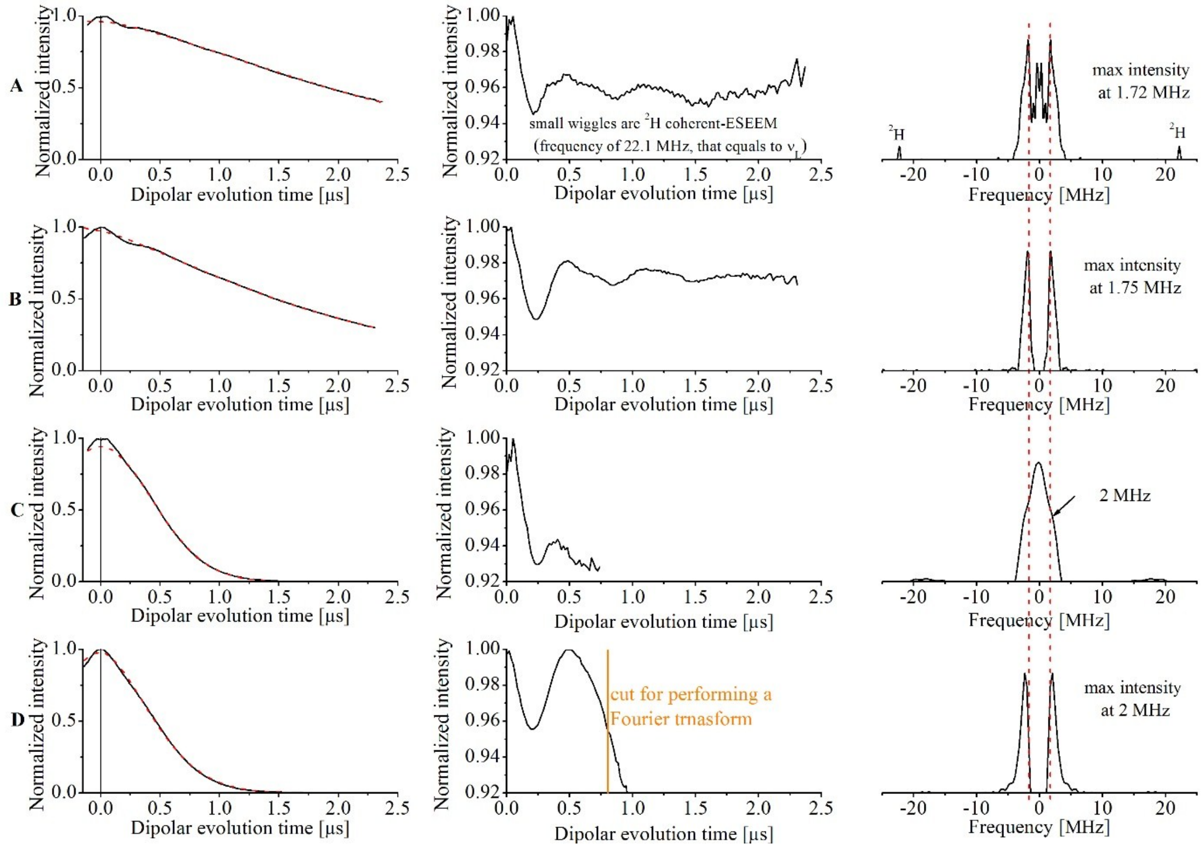

Figure S6. Experimental RIDME time trace, obtained on compound **2** with corresponding stretched exponential background function (left). The time traces were obtained with mixing time of 80 μs. Corresponding background-divided RIDME time trace (middle) and Fourier transform of background-divided time trace (right). **A** Sample in a deuterated solvent and RIDME time trace recorded with hard pulses. **B** Sample in a deuterated solvent and RIDME time trace recorded with soft pulses. **C** Sample in a protonated solvent and RIDME time trace recorded with hard pulses. **D** Sample in a protonated solvent and RIDME time trace recorded with soft pulses.

The RIDME time traces obtained on compound **2** in a protonated solvent decay considerably faster than those obtained in a deuterated solvent. Such a fast decaying backgrounds dampen all kind of oscillations. Therefore, the ambiguity in obtaining of the background function is significant and reliable analysis of the oscillation after background-correction procedure might be not possible. Thus, the background-divided time traces reveal some oscillations with a frequency of about 2 MHz. Due to the uncertainty of obtaining the background functions, this oscillations can correspond with an error of about 0.3 MHz to the ^{14}N, as was discussed above.

6. Relaxation measurements on mono- and bis-MnDOTA complexes at W-band frequencies

Phase memory time measurements (T_{me}) are given in Figure S7. The measurements are performed with standard two-pulse Hahn-echo sequence with hard pulses. Longitudinal electron relaxation time measurements (T_{1e}) are given in Figure S8. Measurements are performed with inversion recovery sequence with hard pulses. The values for T_{1e} are determined as τ_3 - τ_2, where τ_3 and τ_2 are the constants, after which echo decayed by a factor of e^3 and e^2, respectively. Longitudinal relaxation time defined in this way is less affected by spectral diffusion. Due to relatively high error, relaxation times are assumed to be the same for all cases.

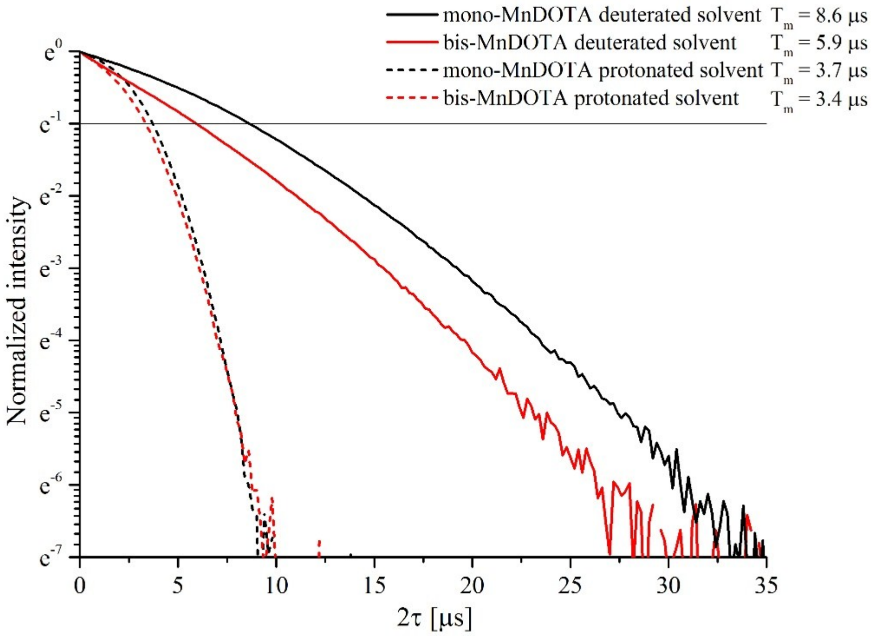

Figure S7. Phase memory time measurements at the spectral position used for RIDME experiments.

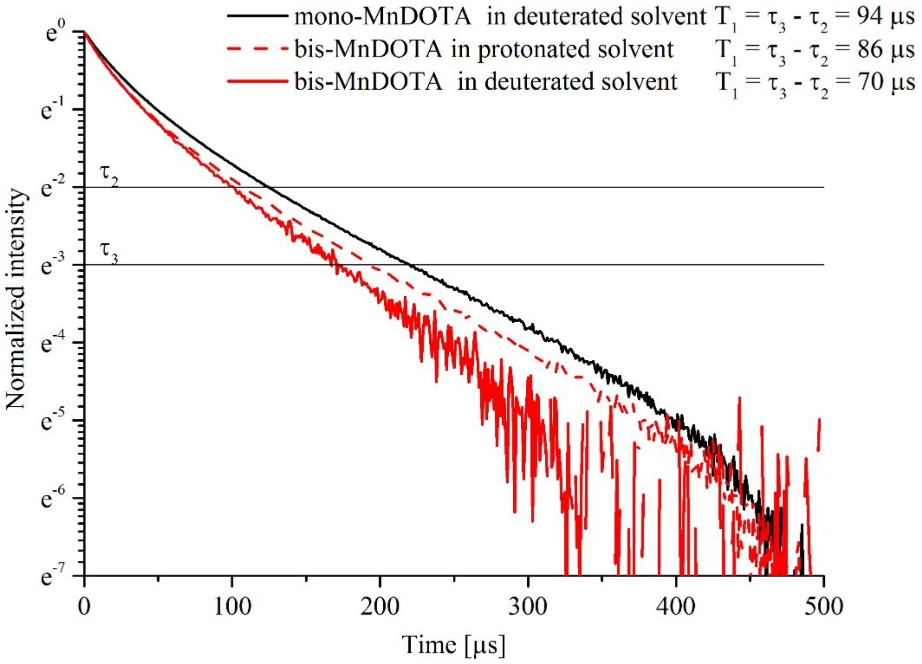

Figure S8. Longitudinal relaxation time measurements at the spectral position used for RIDME experiments.

7. Tikhonov regularization with modified kernel function: influence of the weights of multiple dipolar coupling frequency components

7.1 W-band RIDME with mixing time of 20 μs

Distance distributions obtained with the kernel function for the Tikhonov regularization, where the weight of the first and second harmonic of the dipolar-coupling frequency were varied (parameter β in equation S1) are depicted in Figure S9.

$$K(T,R)=\int_0^1\left[\beta\cos\left(\frac{D_{dd}}{R^3}\left(3x^2-1\right)T\right)+\left(1-\beta\right)\cos\left(2\cdot\frac{D_{dd}}{R^3}\left(3x^2-1\right)T\right)\right]dx \qquad \text{(S1)}$$

Figure S9 shows how the intensity of the peak at 2.0 nm from the second dipolar coupling frequency harmonic, decreases with increasing weight (1 - β) in the kernel function. With the weight β = 0.5 the peak at 2.0 nm disappears and the peak corresponding to the expected distance (2.5 nm) achieves its maximum intensity. When β < 0.5, an additional peak with longer distance appears. This peak roughly corresponds to half the dipolar coupling frequency, as the Tikhonov regularization is now performed with the second term of equation S1 being dominant. The cases where the weight of the second harmonic of the dipolar-coupling frequency exceeds the weight of the first harmonic do not have physical meaning. Such analysis was performed only to observe a tendency in the distance distribution.

Adding the second dipolar coupling frequency harmonic component into the kernel function leads to an increase in the RMSD between the RIDME time trace and corresponding back-calculation. The RMSD map is given in Figure S10. The case where a single peak at the expected distance in the distance distribution was observed (β = 0.5) did not correspond to the minimal RMSD value, although it appeared to be a local minima. Mapping the differences between the background-divided RIDME time trace (also modulation depth scaled) and corresponding back-calculation (see Figure S11 and Fourier transform in Figure S12) showed small amplitude oscillations at all β values. The RMSD values shown in Figure S10 are influenced by these oscillations and cannot be used as a judgment of the fit with different weights of multiple dipolar-coupling frequency components. Such oscillations were not observed with mono-MnDOTA complex. In order to understand the origin of these effects more deeply, a more systematic study is needed.

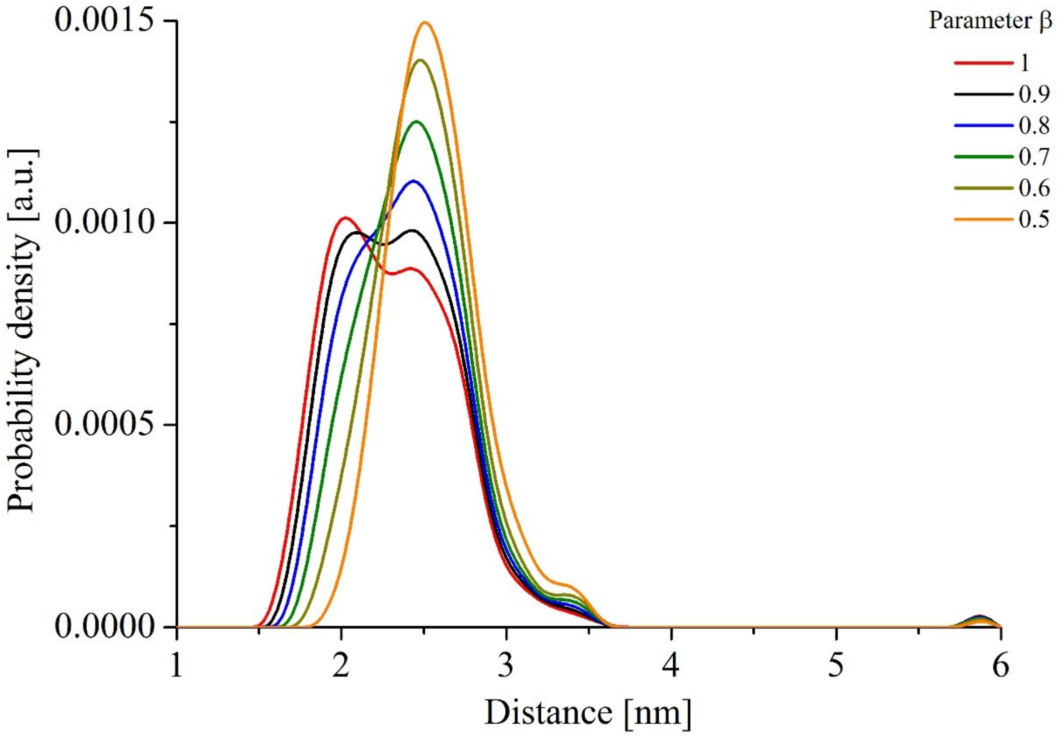

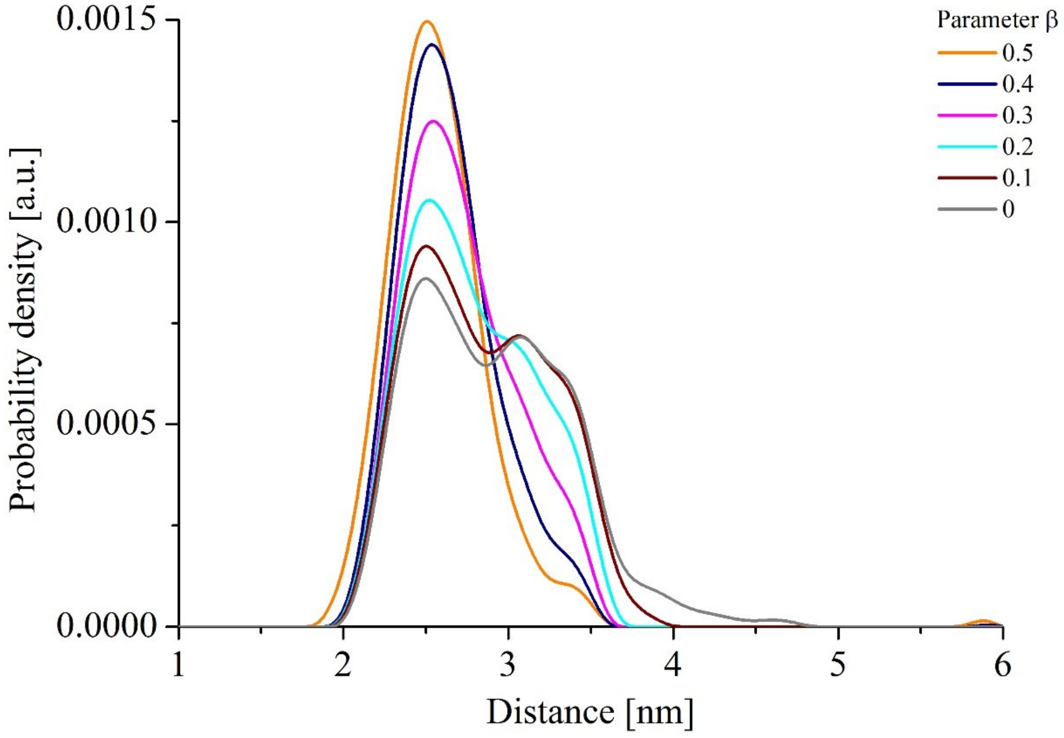

Figure S9. Distance distributions obtained by Tikhonov regularization analysis with the kernel function shown in equation S1 and regularization parameter is 10. Parameter β was varied with a step of 0.1. For better visual comparison the graphs were splitted in two layers. (Top) β is varied in the range [1, 0.5]. (Bottom) β is varied in the range [0.5, 0]. Β of 0.5 is present in both layers as a referential data. Analysis is performed for the RIDME time trace with mixing time of 20 µs obtained on compound **1** in deuterated solvent.

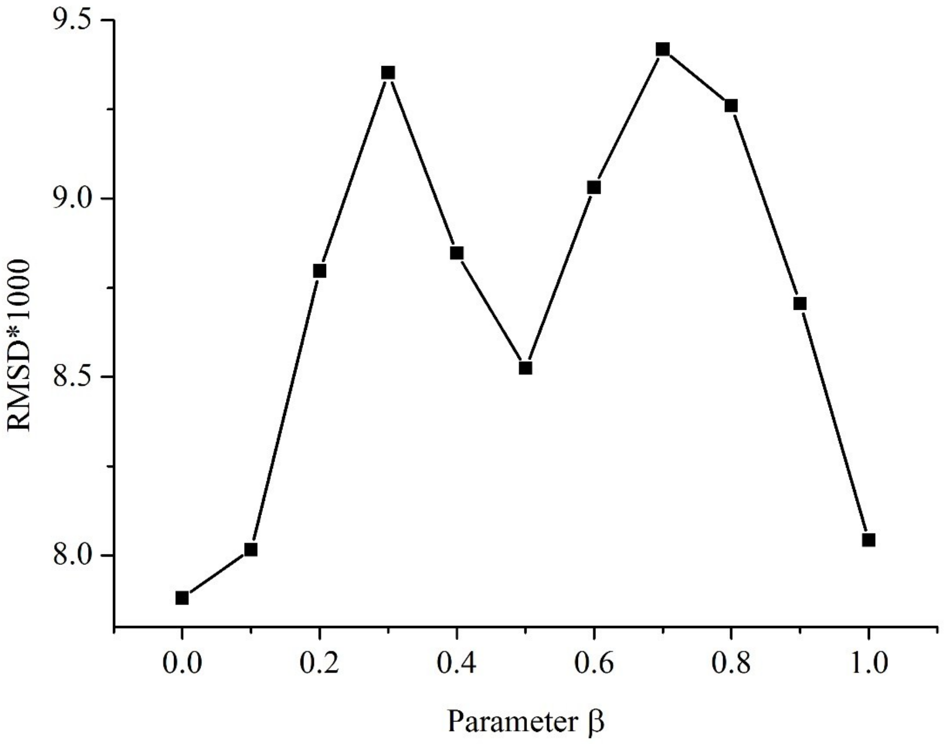

Figure S10. RMSD between modulation depth-scaled RIDME time trace (mixing time of 20 μs, compound **1** in deuterated solvent) and corresponding back-calculation based on Tikhonov regularization analysis with the kernel function shown in equation S1 and regularization parameter is 10.

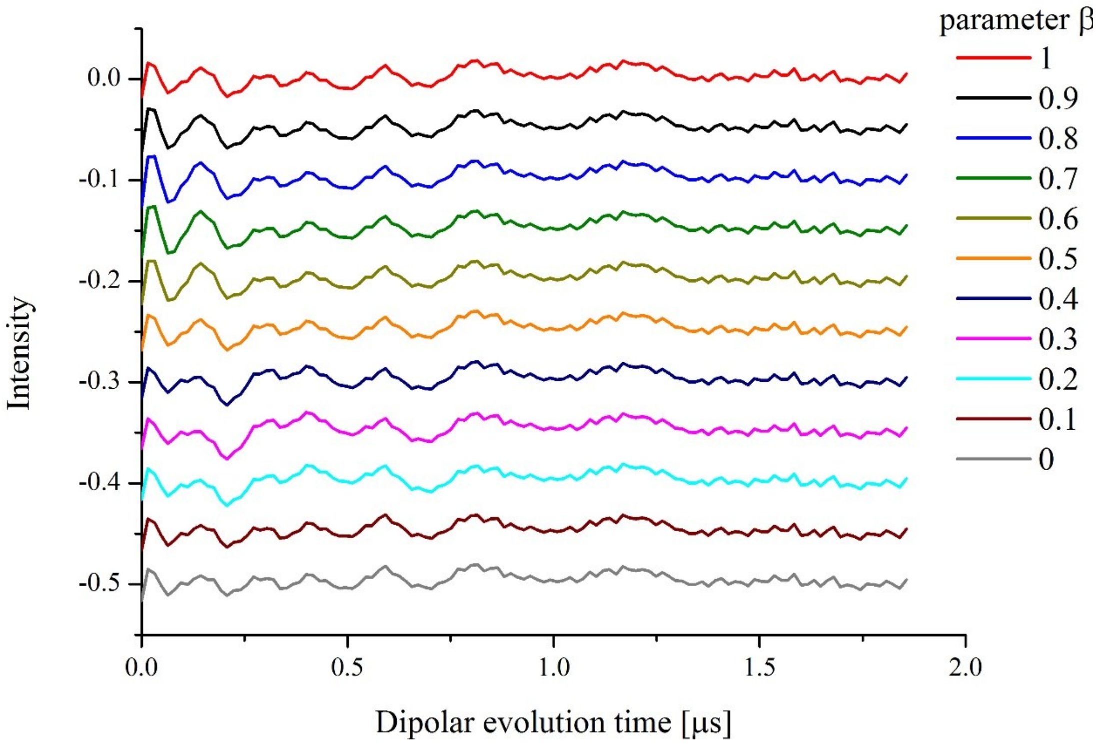

Figure S11. Difference between modulation depth-scaled RIDME time trace (mixing time of 20 μs, compound **1** in deuterated solvent) and corresponding back-calculation based on Tikhonov regularization analysis with the kernel function shown in equation S1 and regularization parameter is 10. All the differences have been vertically offset for better visualization.

The Fourier transforms of the differences (Figure S10) are shown in Figure S11. Several features can be observed in the Fourier transform, as shown in this figure.

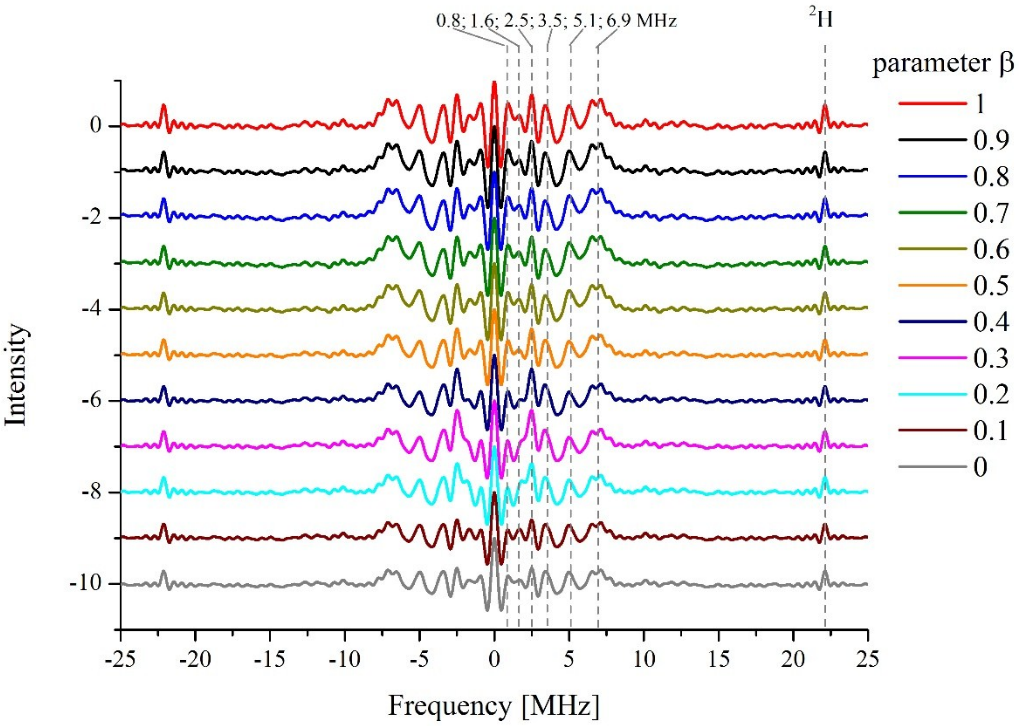

Figure S12. Fourier transform of the difference between modulation depth-scaled RIDME time trace (mixing time of 20 μs, compound **1** in deuterated solvent) and corresponding back-calculation based on Tikhonov regularization analysis with the kernel function shown in equation S1 and regularization parameter is 10. All the Fourier transforms have been vertically offset for better visualization.

7.2 W-band RIDME with mixing time of 80 μs

Distance distributions obtained with the kernel function for the Tikhonov regularization where the weight of the first and second harmonic of the dipolar coupling frequency were varied (parameter β in equation S1) for 80 μs mixing time is depicted in Figure S13. The situation is similar to the case of W-band RIDME time trace with 20 μs mixing time. The RMSD map (Figure S14) is also similar where the RMSD values increase upon adding additional components to the kernel function. The differences between this experimental time trace and back-calculations are depicted in Figure S15 (corresponding Fourier transforms are shown in Figure S16). The features are similar to the previous case, suggesting that the RMSD does not reflect the quality of analysis with different kernel function.

The distance distributions obtained with the kernel function where the weights of the first and second terms were the same, reveals some feature at short distance, which was not the case for 20 μs mixing time (Figure S9). One possible reason for these features could be higher quantum longitudinal relaxation. To account for this, the third harmonic of the dipolar coupling frequency was explicitly included into the kernel function (equation S2), and Tikhonov regularization analysis was performed. Parameter γ reflects the weight for this component. Parameters β' were kept the same and γ was varied from 0 till 0.333, with the step of 0.05 (except for the last case), such that the summed weight of 2β'+ γ equals 1.

$$K(T,R)=\int_0^1\left[\beta'\cos\left(\frac{D_{dd}}{R^3}\left(3x^2-1\right)T\right)+\beta'\cos\left(2\cdot\frac{D_{dd}}{R^3}\left(3x^2-1\right)T\right)+\gamma\cos\left(3\cdot\frac{D_{dd}}{R^3}\left(3x^2-1\right)T\right)\right]dx \quad \text{(S2)}$$

The distance distributions revealed by this analysis is shown in Figure S17 and the differences between experimental time trace (modulation-depth scaled) and corresponding back-calculations are shown in Figure S18 (corresponding Fourier transforms are shown in Figure S19). The RMSD values depending on γ is shown in Figure S20. Whereas the RMSD map contains the minimum at γ value of 0.15 (corresponding of 0.425), and distance distributions obtained with corresponding kernel function lacks the component at about 1.8 nm, this RMSD value is still larger than that revealed by Tikhonov analysis with the conventional kernel function.

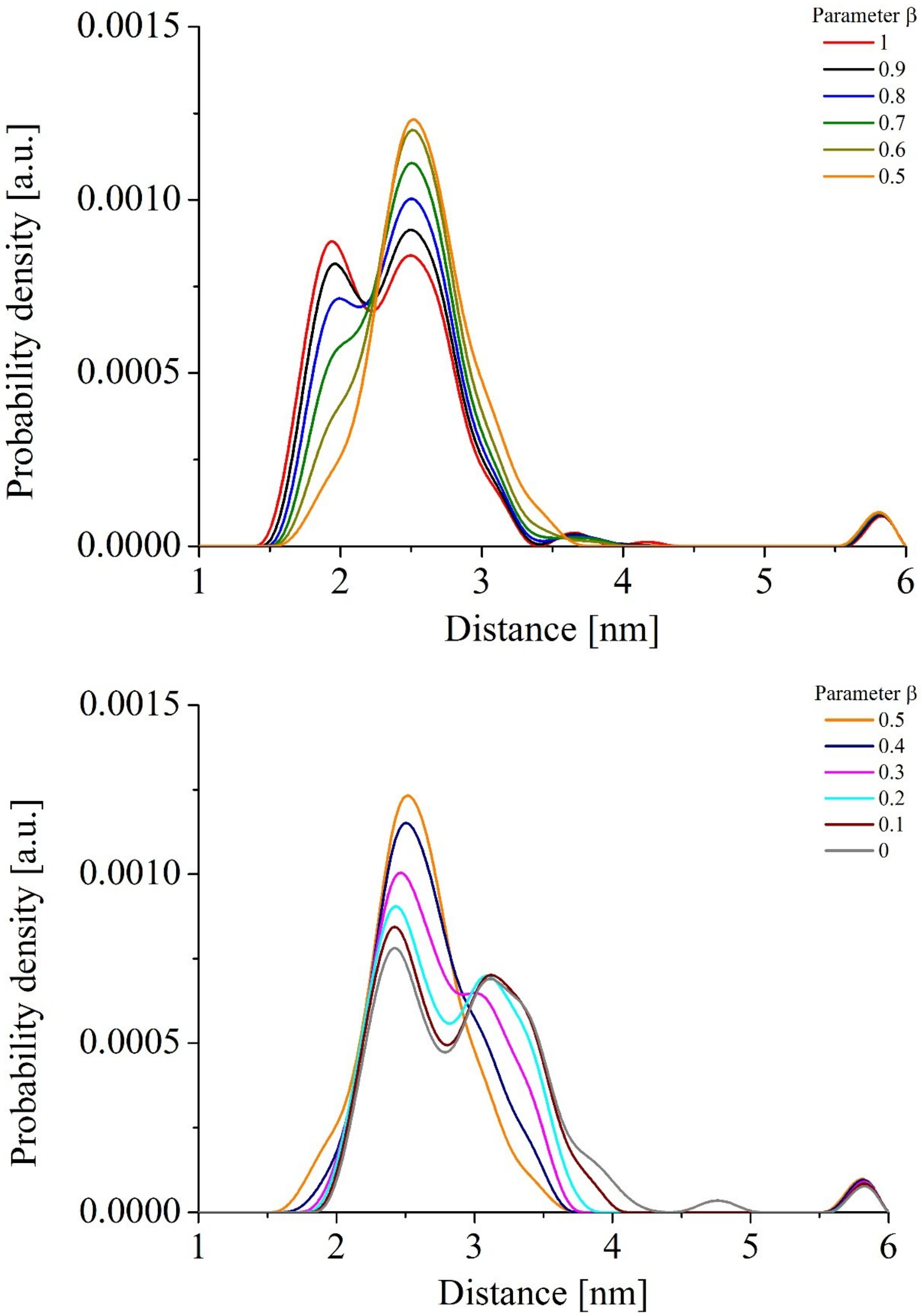

Figure S13. Distance distributions obtained by Tikhonov regularization analysis with the kernel function shown in equation S1 and regularization parameter is 10. Parameter β was varied with a step of 0.1. For better visual comparison the graphs were splitted in two layers. (Top) β is varied in the range [1, 0.5]. (Bottom) β is varied in the range [0.5, 0]. B of 0.5 is present in both layers as a referential data. Analysis is performed for the RIDME time trace with mixing time of 80 µs obtained on compound **1** in deuterated solvent.

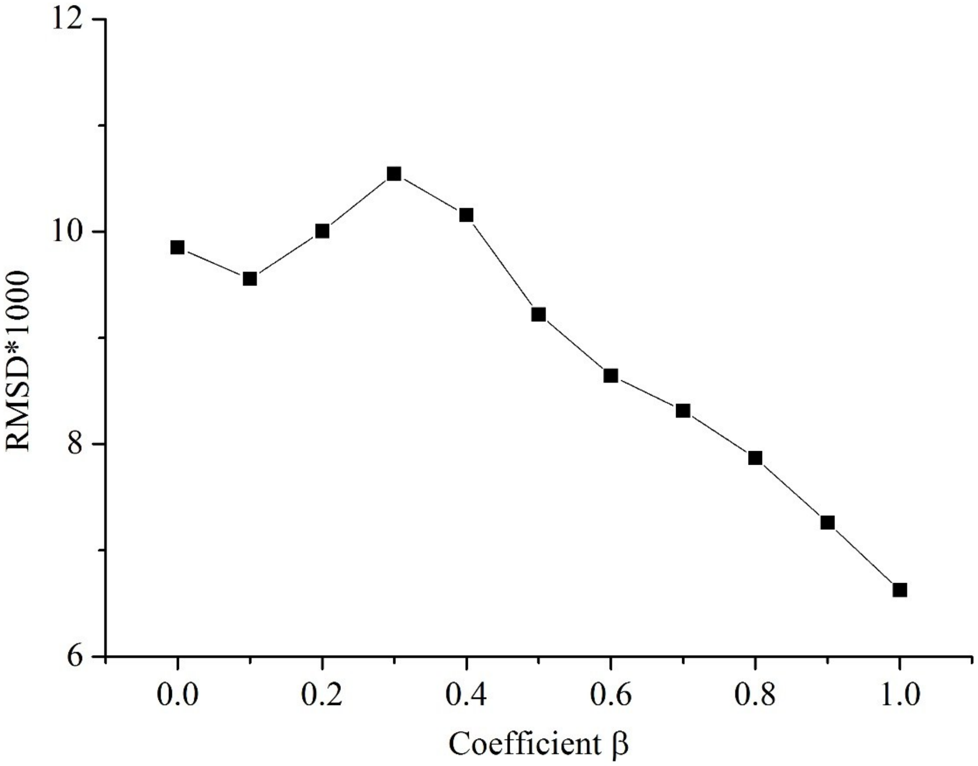

Figure S14. RMSD between modulation depth-scaled RIDME time trace (mixing time of 80 µs, compound **1** in deuterated solvent) and corresponding back-calculation based on Tikhonov regularization analysis with the kernel function shown in equation S1 and regularization parameter is 10.

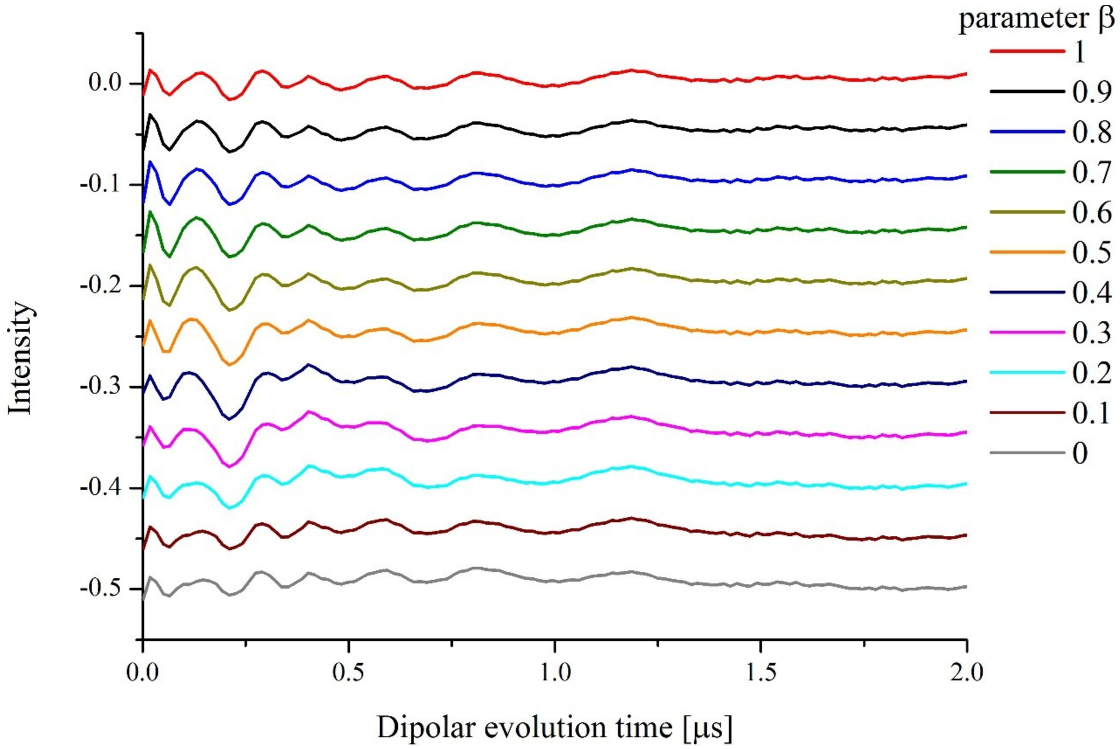

Figure S15. Difference between modulation depth-scaled RIDME time trace (mixing time of 80 µs, compound **1** in deuterated solvent) and corresponding back-calculation based on Tikhonov regularization analysis with the kernel function shown in equation S1 and regularization parameter is 10. All the differences have been vertically offset for better visualization.

The Fourier transforms of the differences, depicted in Figure S15, are shown in Figure S16. The features in the Fourier transform, observed in the previous case, can be also seen in this figure.

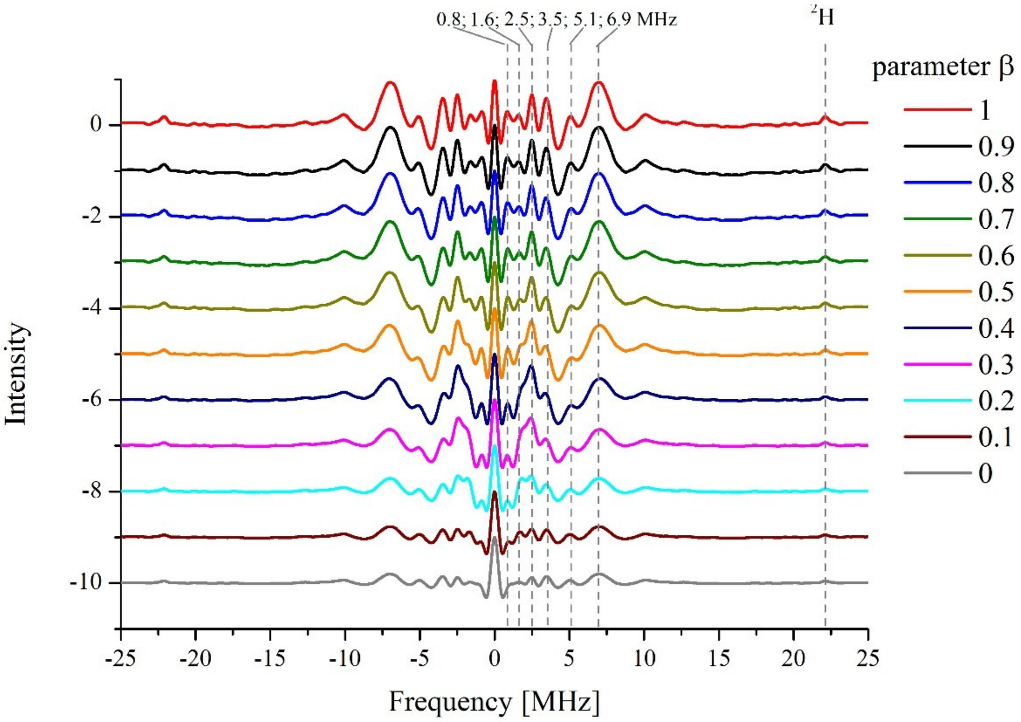

Figure S16. Fourier transform of the difference between modulation depth-scaled RIDME time trace (mixing time of 80 μs, compound **1** in deuterated solvent) and corresponding back-calculation based on Tikhonov regularization analysis with the kernel function shown in equation S1 and regularization parameter is 10. All the Fourier transforms have been vertically offset for better visualization.

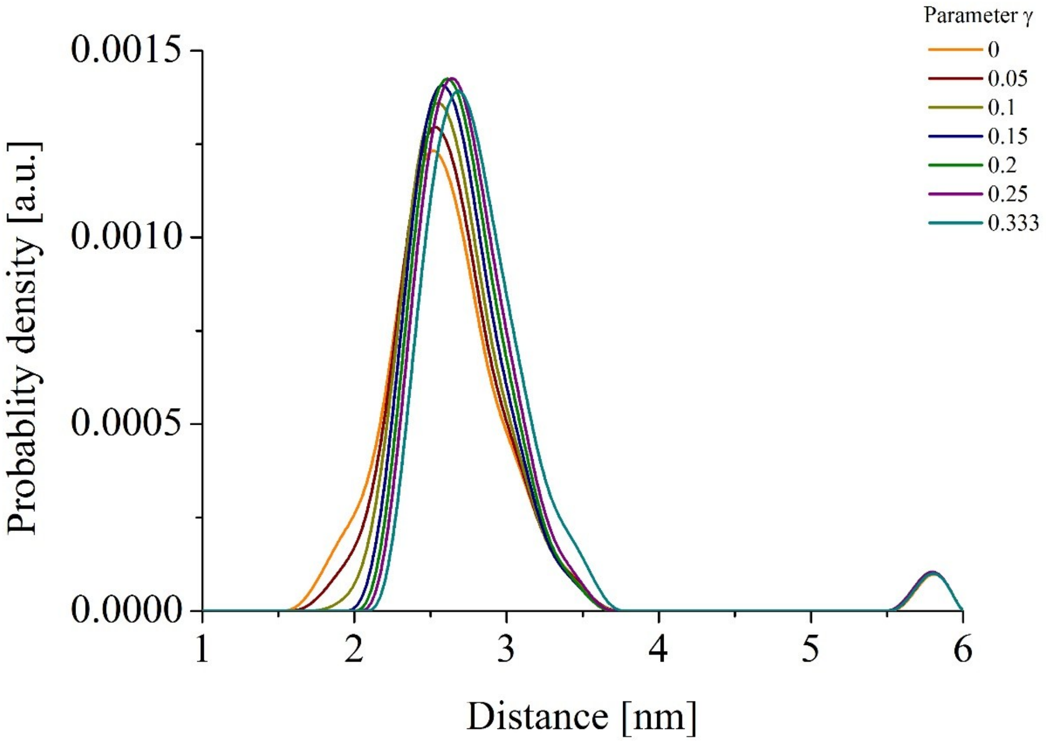

Figure S17. Distance distributions obtained by Tikhonov regularization analysis with the kernel function shown in equation S2 and regularization parameter is 10. Parameter γ was varied with a step of 0.05. Analysis is performed for the RIDME time trace with mixing time of 80 μs obtained on compound **1** in deuterated solvent.

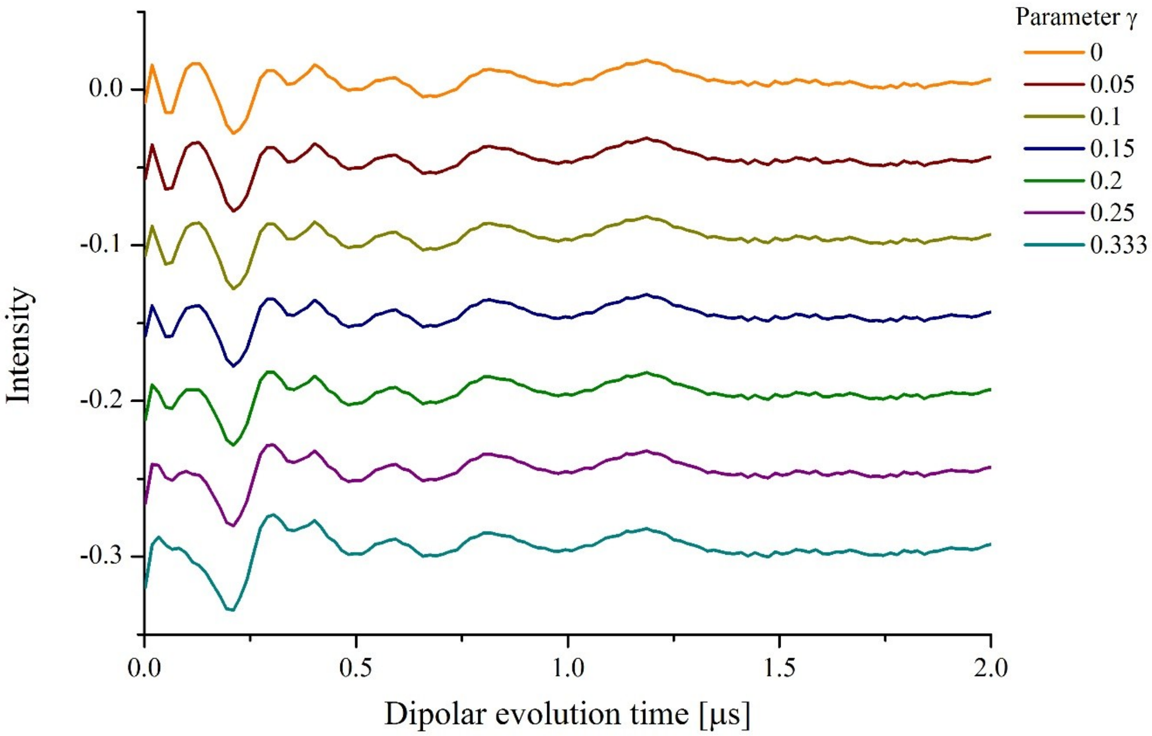

Figure S18. Difference between modulation depth-scaled RIDME time trace (mixing time of 80 µs, compound **1** in deuterated solvent) and corresponding back-calculation based on Tikhonov regularization analysis with the kernel function shown in equation S2 and regularization parameter is 10. All the differences have been vertically offset for better visualization.

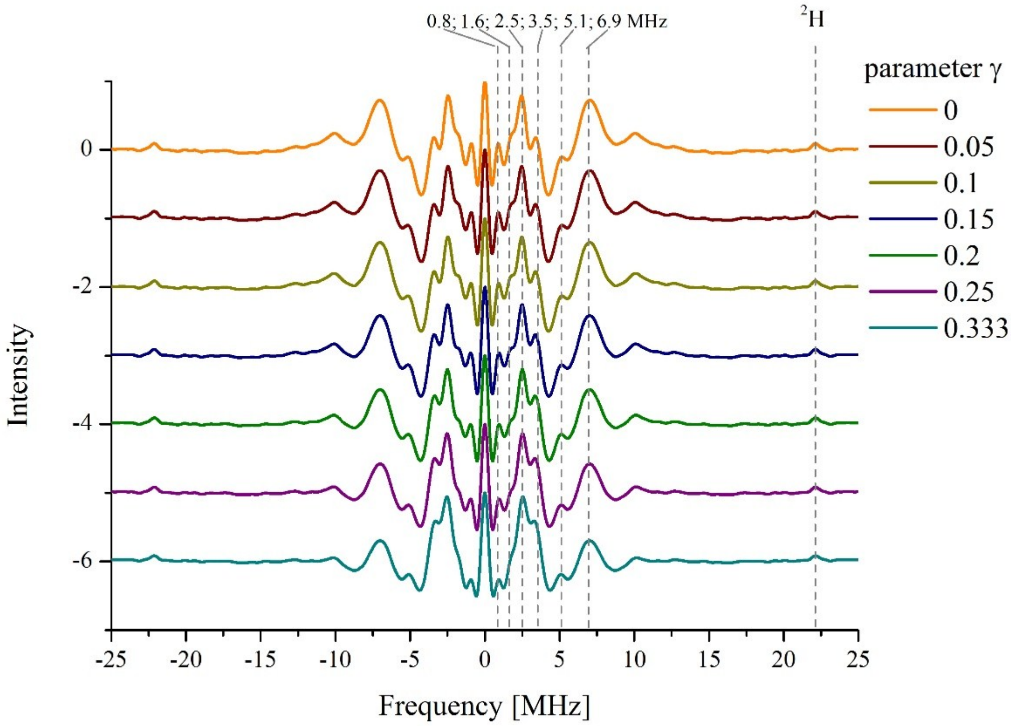

Figure S19. Fourier transform of the difference between modulation depth-scaled RIDME time trace (mixing time of 80 µs, compound **1** in deuterated solvent) and corresponding back-calculation based on Tikhonov regularization analysis with the kernel function shown in equation S2 and regularization parameter is 10. All the Fourier transforms have been vertically offset for better visualization.

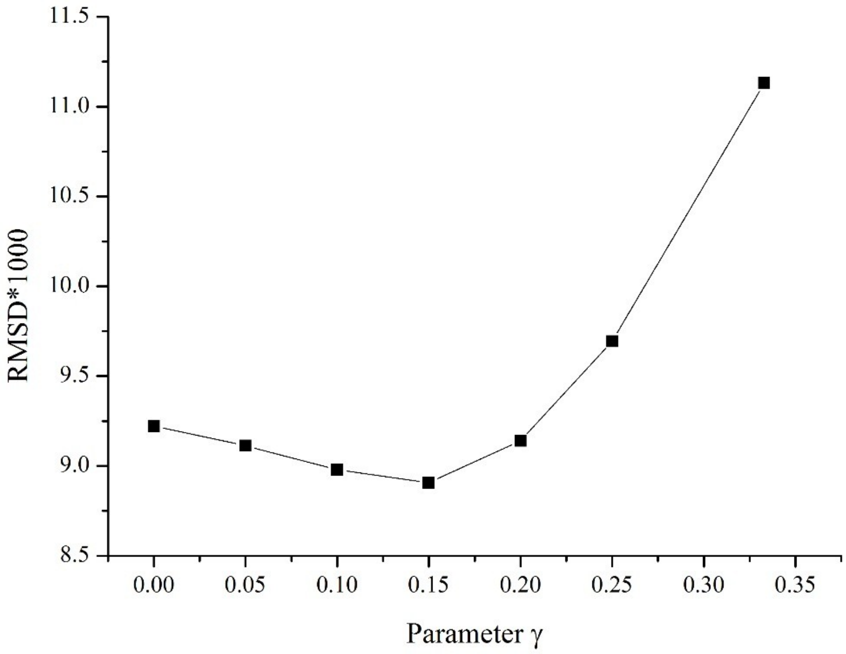

Figure S20. RMSD between modulation depth-scaled RIDME time trace (mixing time of 80 μs, obtained on compound **1** in deuterated solvent) and corresponding back-calculation based on Tikhonov regularization analysis with the kernel function shown in equation S2 and regularization parameter is 10.

7.3 J-band RIDME with mixing time of 30 μs

Distance distributions obtained with the kernel function for the Tikhonov regularization where the weight of the first and second harmonic of the dipolar coupling frequency were varied (parameter β in equation S1) for J-band RIDME time trace is depicted in Figure S21. The corresponding map of RMSD between J-band RIDME time trace (mixing time of 30 μs) and back-calculations is depicted in Figure S22. The differences between corresponding time traces are given in Figure S23 (corresponding Fourier transforms are shown in Figure S24). Again the RIDME maps featured oscillations that were every similar to the W-band data. Taking into account this and the fact that RIDME on mono-MnDOTA complex does not reveal these oscillations, might suggest that they are not experimental artefacts and are specific to the RIDME on compound **1**. However, the frequency for these oscillations do not correspond to the hyperfine couplings to ^{14}N or ^{1}H.

The possible origins of the wing from about 3 to 4 nm in the distance distributions is given in the next section. As is the case of W-band RIDME time traces with the mixing time of 80 μs, the J-band distance distributions obtained with kernel function with $\beta = 0.5$ shows small peaks at about 1.8 nm. Therefore, as in the case with the W-band RIDME time trace, the analysis is also performed using Tikhonov regularization with the kernel function, given in equation S2, where the third dipolar-coupling frequency harmonic is added. The distance distributions, differences between experimental time traces and back-calculations with corresponding Fourier transforms and the RMSD map is presented in Figures S25-S28, respectively. As in the W-band RIDME (80 μs mixing time) case, the small intensity peak disappears with increasing γ. And with the value 0.15 the minimum of RMSD was achieved, which is still, however, larger than that obtained with conventional kernel function.

We conclude that RMSD values between RIDME time traces and back-calculations for both frequencies are influenced to a significant extent by oscillations, the origin of those are not completely understood. Therefore, RMSD is not a good criteria for choosing proper weights of first-, second- and third dipolar-coupling frequency harmonics.

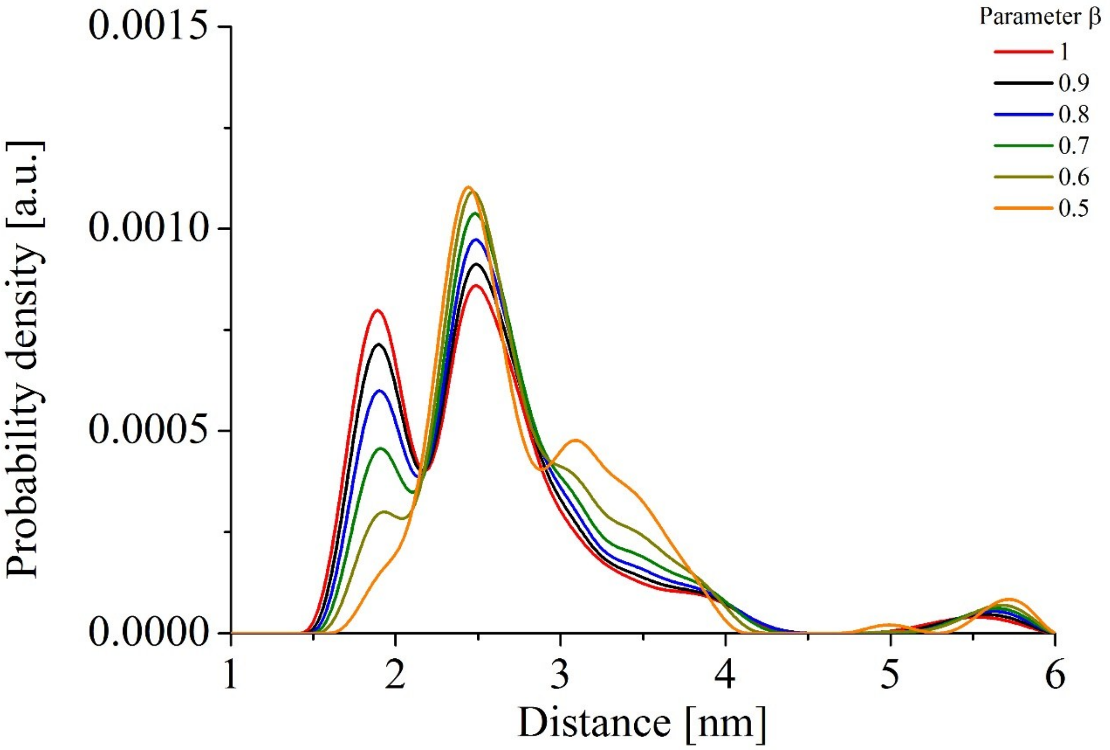

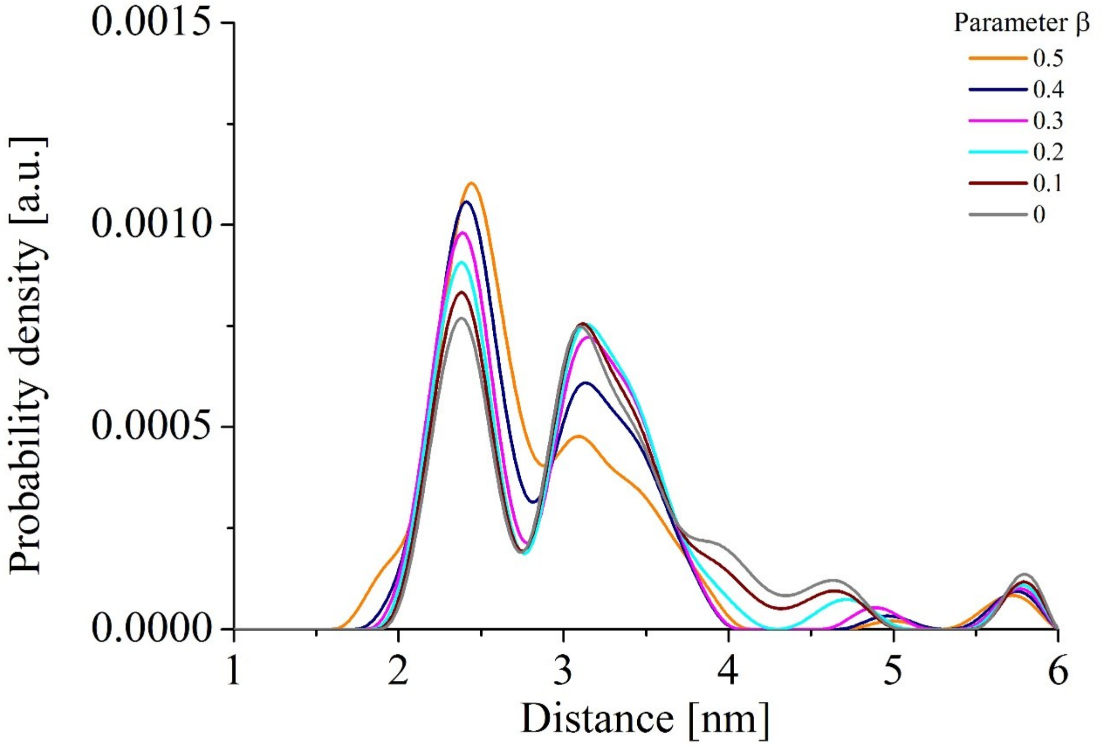

Figure S21. Distance distributions obtained by Tikhonov regularization analysis with the kernel function shown in equation S1 and regularization parameter is 10. Parameter β was varied with a step of 0.1. For better visual comparison the graphs were splitted in two layers. (Top) β is varied in the range [1, 0.5]. (Bottom) β is varied in the range [0.5, 0]. B of 0.5 is present in both layers as a referential data. Analysis is performed for the J-band RIDME time trace with mixing time of 30 μs obtained on compound **1** in deuterated solvent.

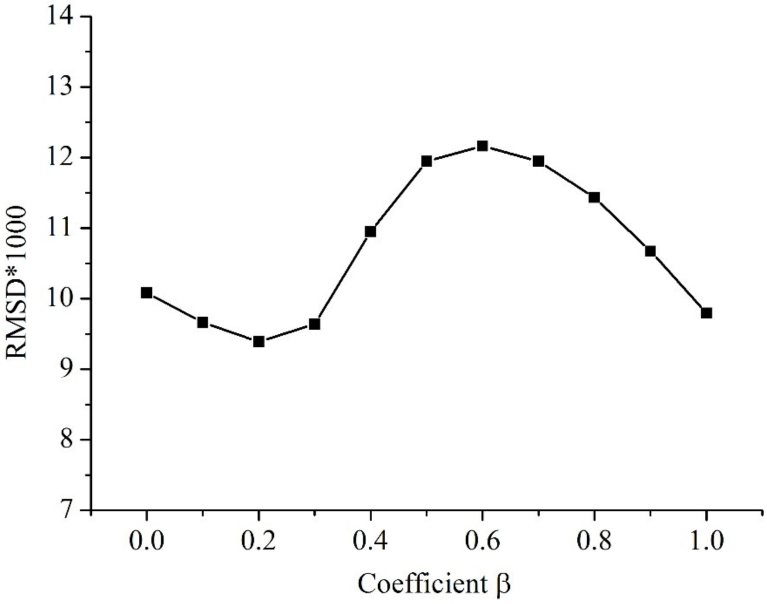

Figure S22. RMSD between modulation depth-scaled J-band RIDME time trace (mixing time of 30 μs, compound **1** in deuterated solvent) and corresponding back-calculation based on Tikhonov regularization analysis with the kernel function shown in equation S1 and regularization parameter is 10.

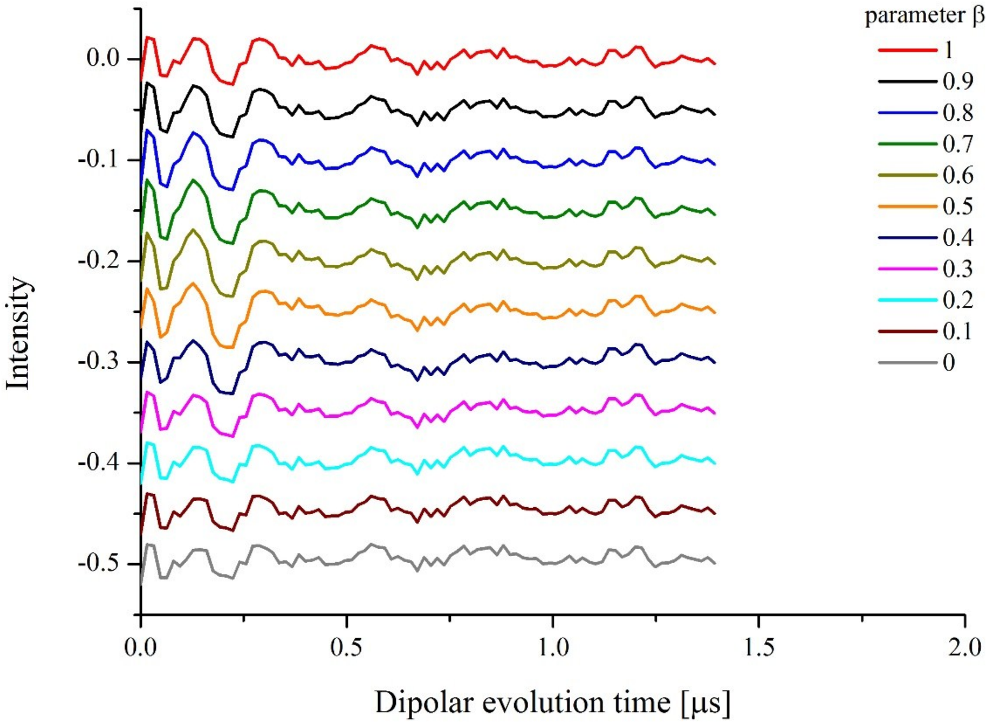

Figure S23. Difference between modulation depth-scaled J-band RIDME time trace (mixing time of 30 μs, compound **1** in deuterated solvent) and corresponding back-calculation based on Tikhonov regularization analysis with the kernel function shown in equation S1 and regularization parameter is 10. All the differences have been vertically offset for better visualization.

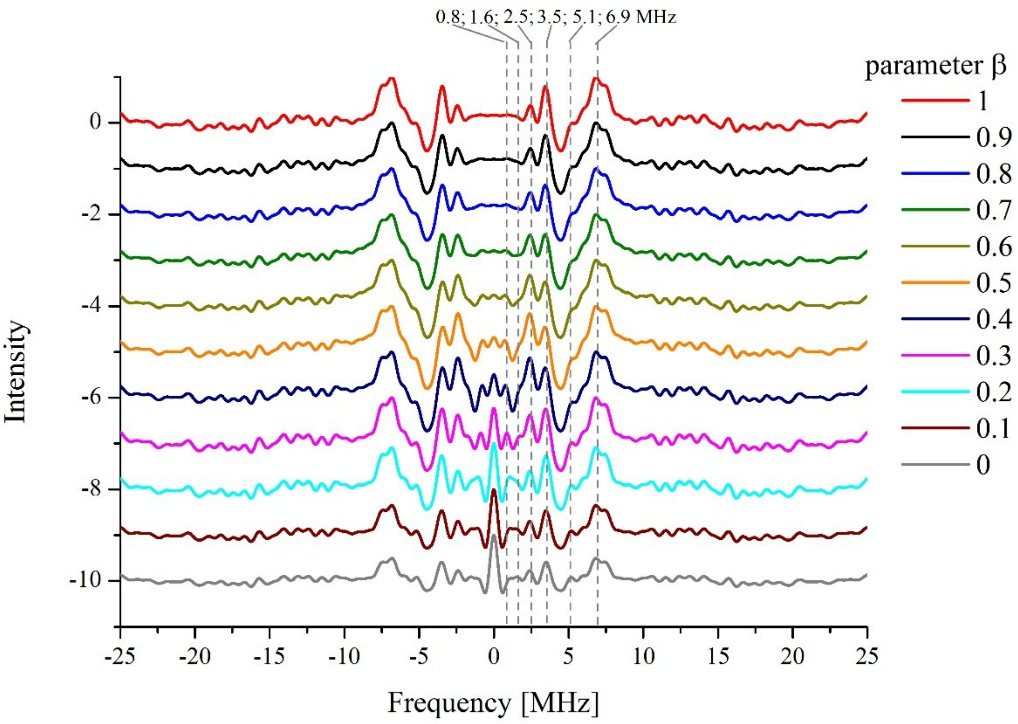

Figure S24. Fourier transform of the difference between modulation depth-scaled J-band RIDME time trace (mixing time of 30 μs, compound **1** in deuterated solvent) and corresponding back-calculation based on Tikhonov regularization analysis with the kernel function shown in equation S1 and regularization parameter is 10. All the Fourier transforms have been vertically offset for better visualization.

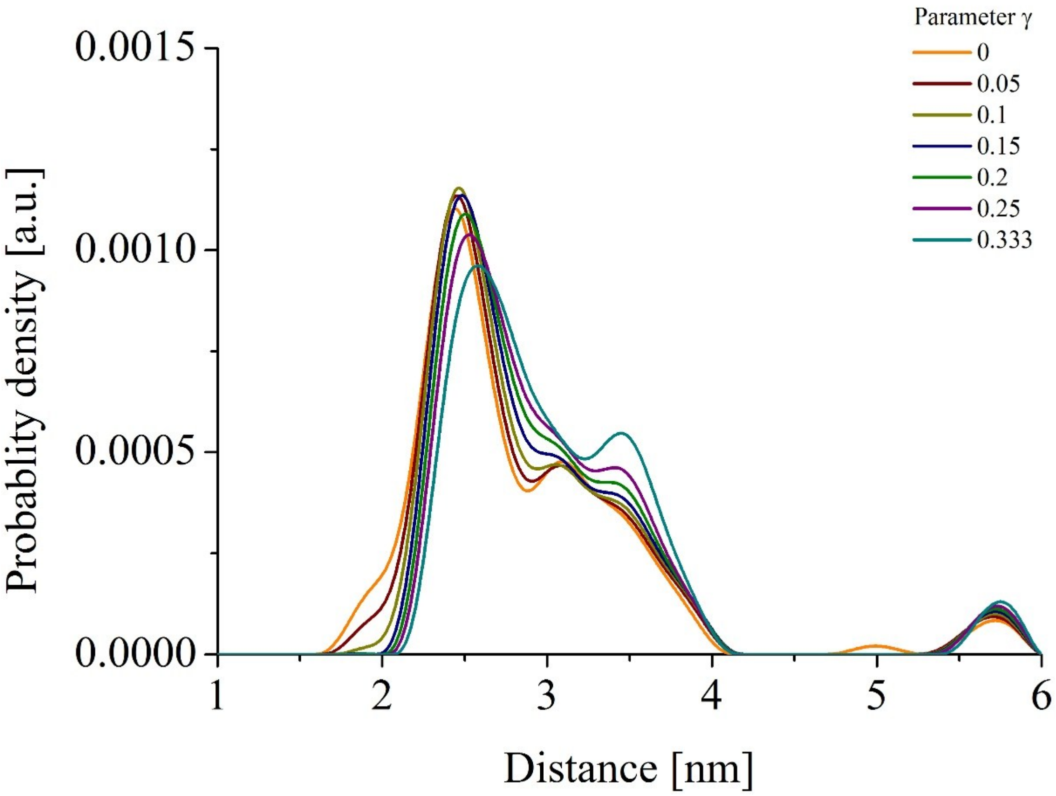

Figure S25. Distance distributions obtained by Tikhonov regularization analysis with the kernel function shown in equation S2 and regularization parameter is 10. Parameter γ was varied with a step of 0.05. Analysis is performed for the J-band RIDME time trace with mixing time of 30 μs obtained on compound **1** in deuterated solvent.

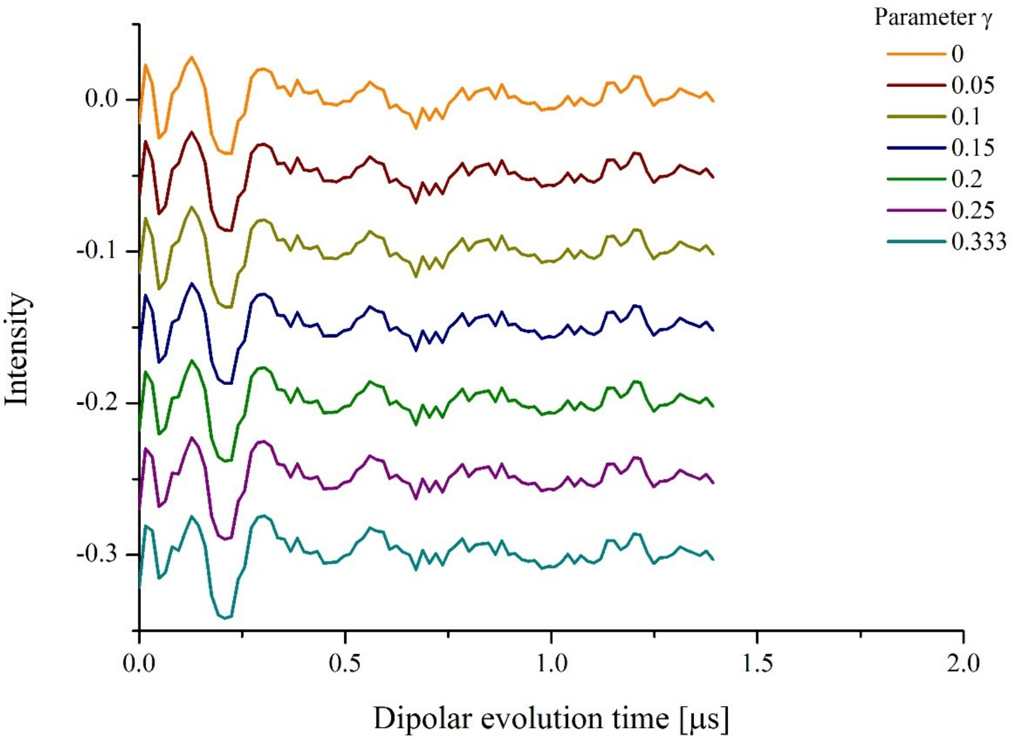

Figure S26. Difference between modulation depth-scaled J-band RIDME time trace (mixing time of 30 μs, compound **1** in deuterated solvent) and corresponding back-calculation based on Tikhonov regularization analysis with the kernel function shown in equation S2 and regularization parameter is 10. All the differences have been vertically offset for better visualization.

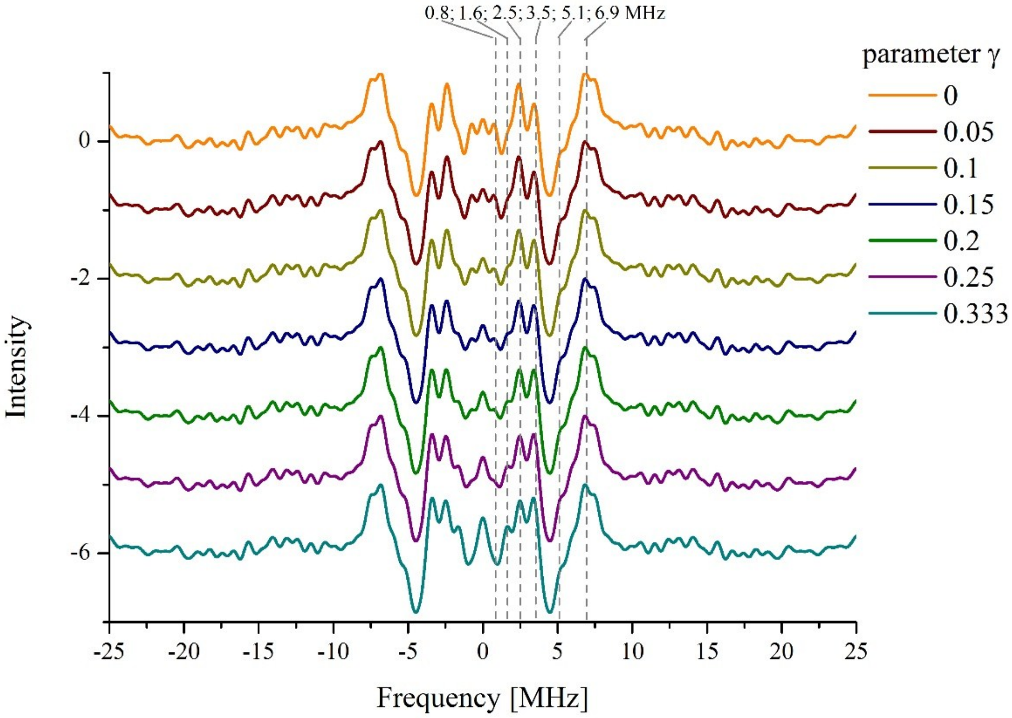

Figure S27. Fourier transform of the difference between modulation depth-scaled J-band RIDME time trace (mixing time of 30 μs, compound **1** in deuterated solvent) and corresponding back-calculation based on Tikhonov regularization analysis with the kernel function shown in equation S2 and regularization parameter is 10. All the Fourier transforms have been vertically offset for better visual representation.

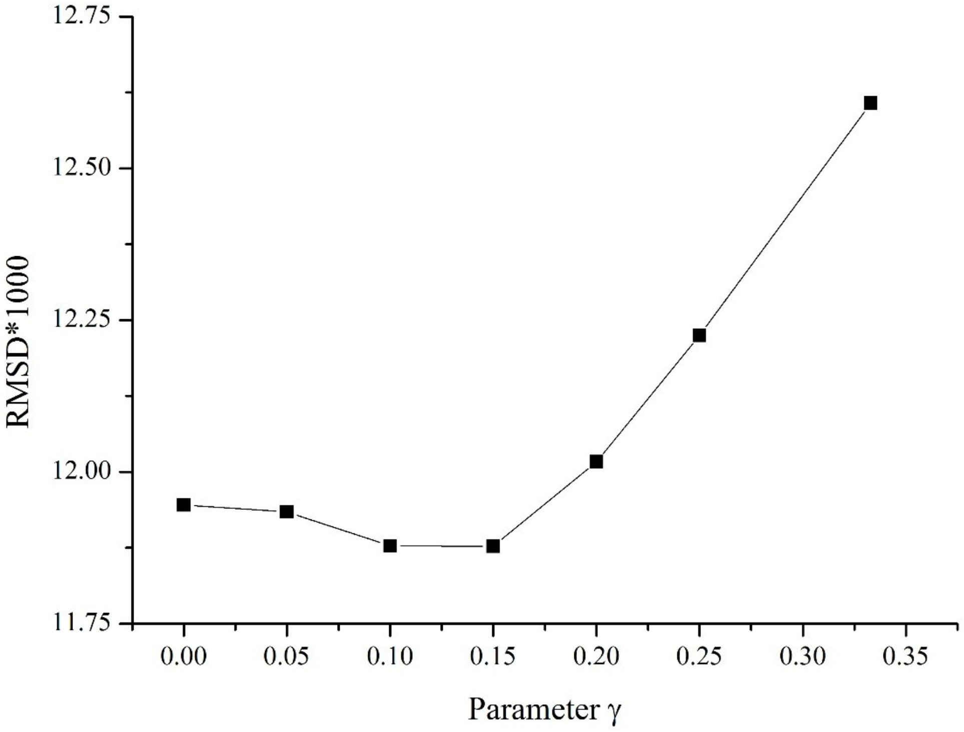

Figure S28. RMSD between modulation depth-scaled J-band RIDME time trace (mixing time of 30 μs, compound **1** in deuterated solvent) and corresponding back-calculation based on Tikhonov regularization analysis with the kernel function shown in equation S2 and regularization parameter is 10.

8. Wing from 3 to 4 nm in the distance distribution corresponded to J-band RIDME time trace

Five-pulse RIDME is a single frequency dipolar spectroscopy experiment. To record the undistorted initial part of the time trace, an 8-step phase-cycle is needed to cancel moving Hahn echo from the last two pulses and the refocused stimulated echo which originates from all five pulses.[4] W-band RIDME experiments were performed on the EPR spectrometer with 4-fixed and power/phase - calibrated microwave channels, whereas the phases in the J-band spectrometer were generated with an arbitrary waveform generator (AWG). If the phases are not set perfectly, the cancelling of both echo signals is not 100% efficient, which can distort the initial part of the RIDME time trace. Fourier transform of the background-divided J-band RIDME time trace (Figure S29 B) reveals an intense zero-frequency component, which was not observed for the W-band RIDME time traces (see Figure S30). Tikhonov regularization of this time trace reveals a wing from 3 to 4 nm in the distance distribution, which becomes significantly more intense upon modification of the kernel function (see Figure 6I). To test the effect of the intense zero-frequency component seen in the Fourier transform, additional stretched exponential function was subtracted from the background-divided J-band RIDME trace as a baseline (see Figure S29 A). This baseline function was fitted such that the zero-frequency component in the Fourier transform of the resulted time trace disappears. The resultant baseline function and the corrected RIDME time trace as well as the Fourier transforms of background-divided and additionally baseline corrected time traces are depicted in Figure S29 A and S29 B. Comparison of the Fourier transforms of both W-band RIDME time traces with the Fourier transform of the baseline corrected J-band time trace is given in Figure S30 B. Tikhonov regularization analysis of the baseline-corrected RIDME time trace with the conventional and modified kernel functions (see equations 4 and 5 in the main text) is given in Figure S29 C and S29 D. As can be seen from Figure S29 D, the distance distributions yielded by Tikhonov analysis with conventional kernel function does not contain such a prominent wing from 3 to 4 nm compared to analysis of the J-band RIDME time trace (Figure 6I).

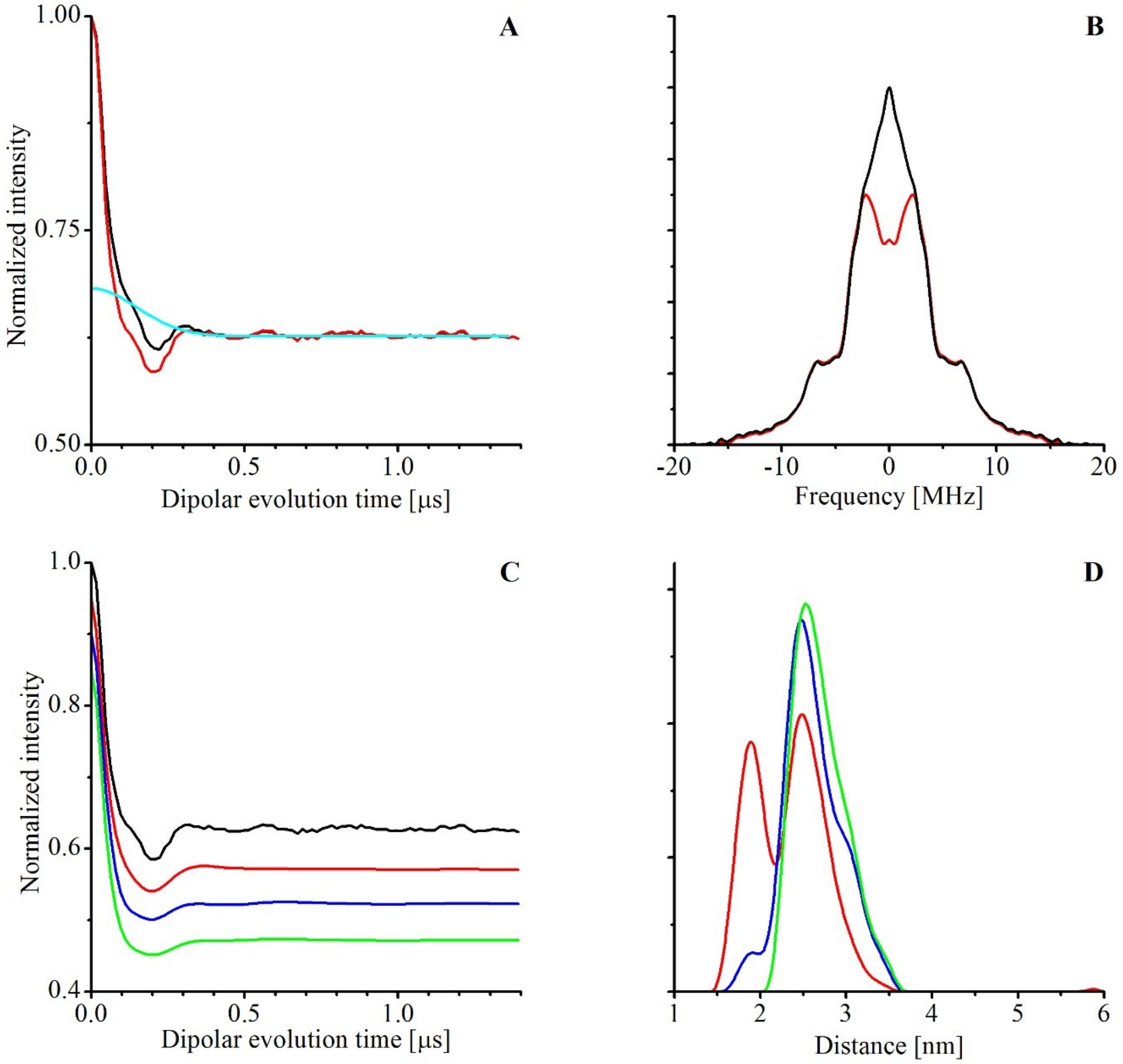

Figure S29. **(A)** The 25 K background-divided RIDME time trace on compound **1** in deuterated solvent obtained at J-band frequencies with mixing time of 30 μs (black, from Figure 6F), stretched-exponential baseline (cyan) and baseline-subtracted RIDME time trace (red). **(B)** Fourier transform of the J-band background-divided RIDME time trace (black, from Figure 6F) and of the baseline subtracted background-divided RIDME time trace (red). **(C)** The baseline-subtracted background-divided RIDME time trace (black) with corresponding fits based on Tikhonov regularization analysis with standard single-frequency component kernel function (red); equally-weighted single- and double-frequency components (0.5 each) modified kernel function (blue); and equally-weighted single- and double-frequency components (0.425 each) with additional triple-frequency component (0.15) modified kernel function (green). Tikhonov regularization was performed using an in-house program with the regularization parameters set to 10 for all fitting procedures. **(D)** The corresponding distance distributions obtained from the Tikhonov regularizations using the different kernel functions.

9. W-band RIDME time traces with 20 and 80 μs mixing times, the time traces obtained as a division, corresponding Fourier transforms and J-band time trace

The W-band RIDME time traces with corresponding Fourier transforms are depicted in Figure S30.

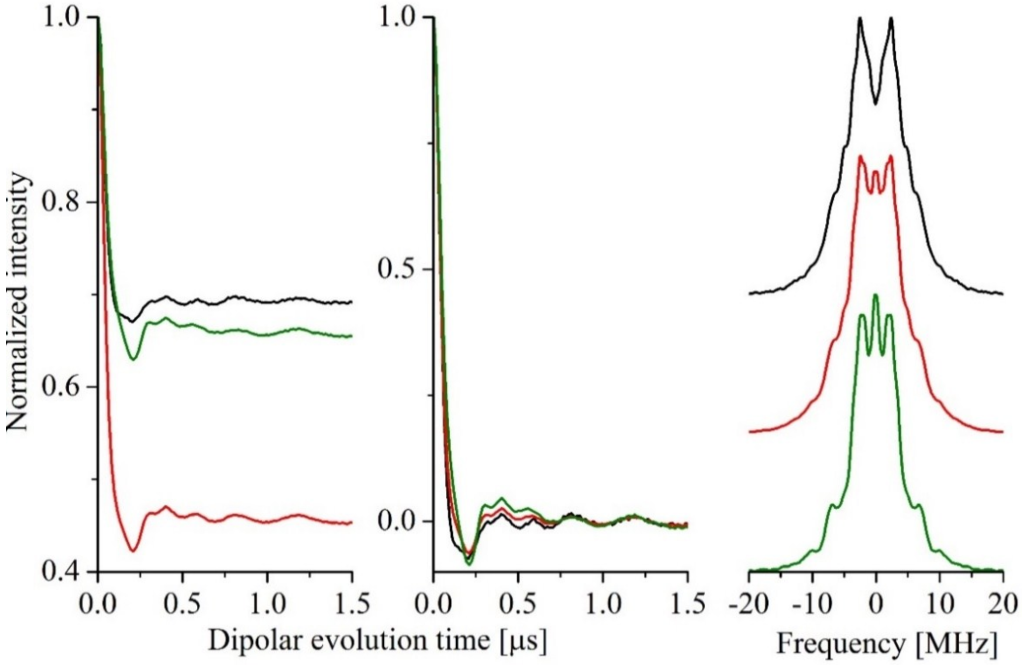

Figure S30 A. **Left**. W-band RIDME time traces on compound **1** in deuterated solvent obtained with 20 μs (black), 80 μs (red) mixing times and their divison (green). **Middle**. Modulation depth scaled RIDME time traces. **Right**. Corresponding Fourier transforms.

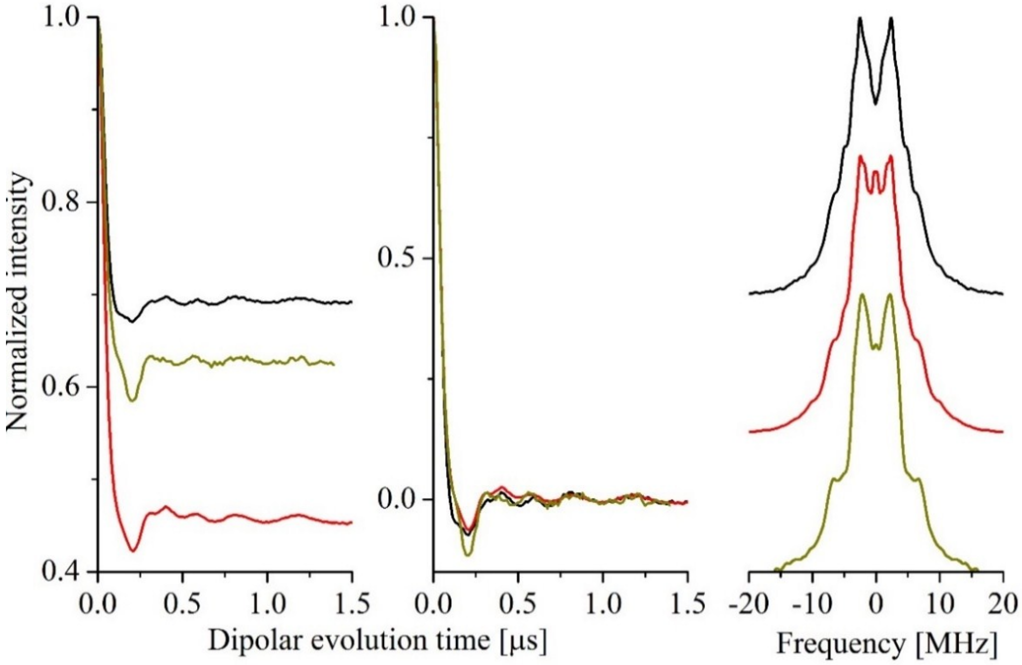

Figure S30 B. **Left**. W-band RIDME time traces on compound **1** in deuterated solvent obtained with 20 μs (black), 80 μs (red) mixing times and corrected J-band RIDME time trace with 30 μs mixing time (dark gold). **Middle**. Modulation depth scaled RIDME time traces. **Right**. Corresponding Fourier transforms.

10. Comparison of electron spin relaxation times at W- and J-band frequencies

Electron spin relaxation time measurements are given in Figures S31 (T_{1e}) and S32 (T_{me}).

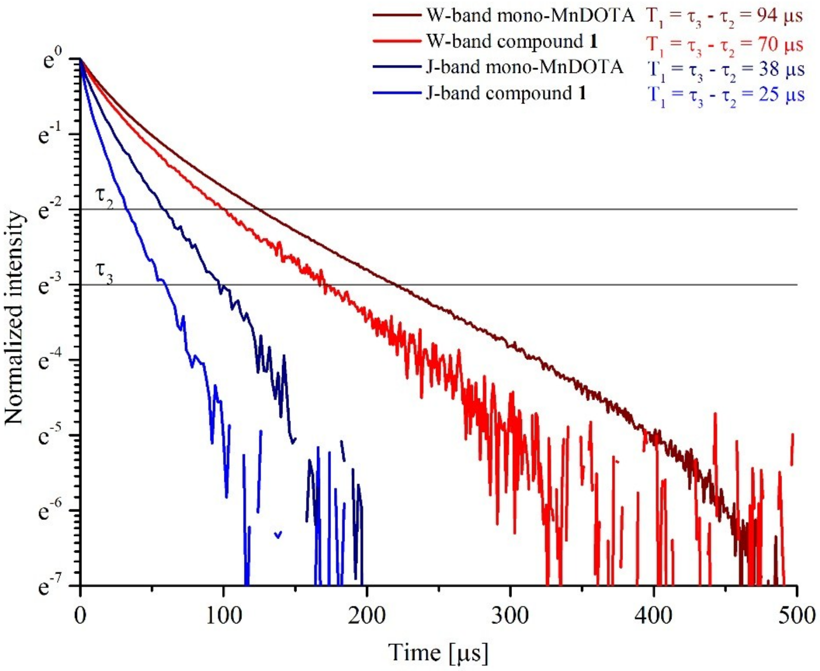

Figure S31. Longitudinal relaxation time measurements on compound **1** and mono-MnDOTA complexes in deuterated solvent at 25K at W- and J-band frequencies. At W- and J-band inversion and saturation recovery (1ms saturation pulse) sequences were used. Spectral position was the highest field hyperfine component.

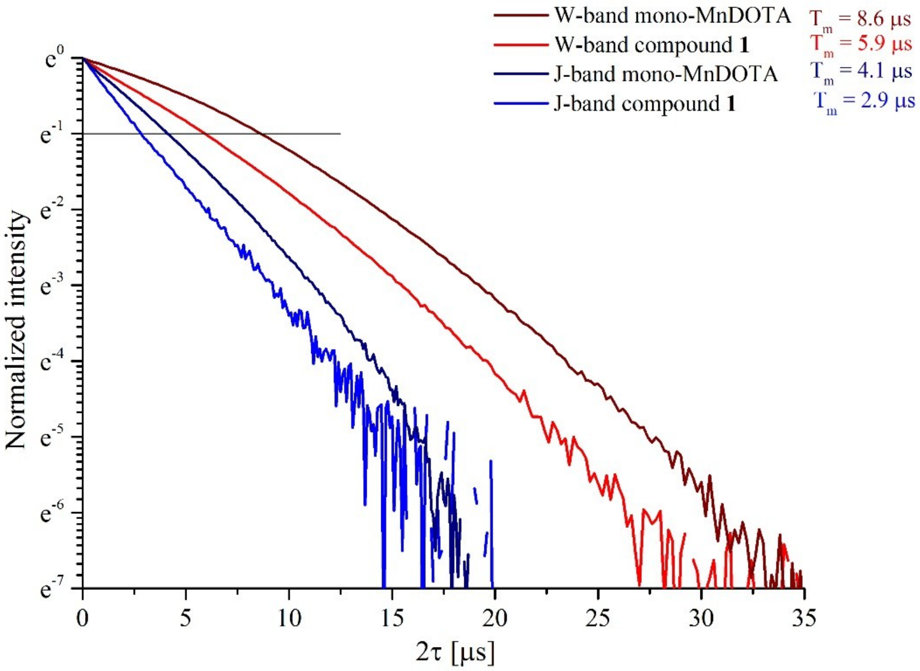

Figure S32. Phase memory time measurements on compound **1** and mono-MnDOTA complexes in deuterated solvent at 25K at W- and J-band frequencies. Hahn-echo sequence were used. Spectral position was the highest field hyperfine component.

11. Comparison of the distance distributions corresponding to different experiments

Distance distributions obtained by Tikhonov regularization analysis of different dipolar spectroscopy experiments are depicted in Figure S33.

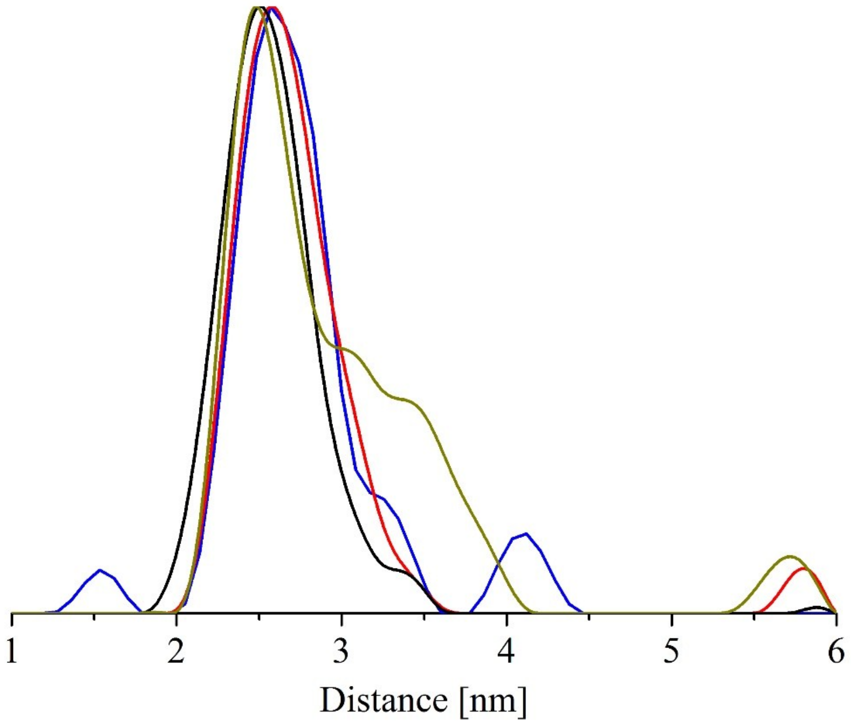

Figure S33. Distance distributions obtained with Tikhonov regularization of PELDOR time trace with 70 MHz pump-probe frequency offset (blue), W-band RIDME time trace obtained with a mixing time of 20 μs with the modified kernel function (equation 4 in the main text) (black), W-band RIDME time trace obtained with a mixing time of 80 μs with the modified kernel function (equation 5) (red), J-band RIDME time trace obtained with a mixing time of 30 μs with the modified kernel function (equation 5) (dark gold). All distance distributions correspond to compound **1** in deuterated solvent. Regularization parameter for all distance distributions was 10. Tikhonov analysis for PELDOR was performed with DeerAnalysis toolbox and for RIDME time traces with in-house program.

12. Broad distance distributions measured by RIDME

In order to model a situation in which RIDME experiments are performed on a relatively flexible system, such that Tikhonov regularization analysis with conventional kernel function would give a single peak, because the first and second harmonics of the dipolar coupling cannot be easily distinguished, the Gaussian distance distribution with the most probable distance of 4 nm and a full-width at half maximum of 1.5 nm was generated (Figure S34 C, black). Based on this distance distribution, the RIDME time trace, where single and double dipolar coupling frequency components have the equal weights of 0.5, was generated (Figure S34, A black). Tikhonov regularization analysis on this RIDME time trace was performed with different kernel functions. Analysis with the conventional kernel function reveals a peak in the distance distribution with a shifted most probable distance (15% shift with respect to the expected distance of 4 nm) (Figure S34 C, red). However, Tikhonov analysis with the modified kernel function (see equation 4 in the main text) reveals a distance distribution, which is almost exactly the same, as was used to generate the RIDME time trace (Figure S34 C, green). The back-calculated time traces and the differences between the generated RIDME time trace and the back-calculations are depicted in Figure S34 A and B, respectively.

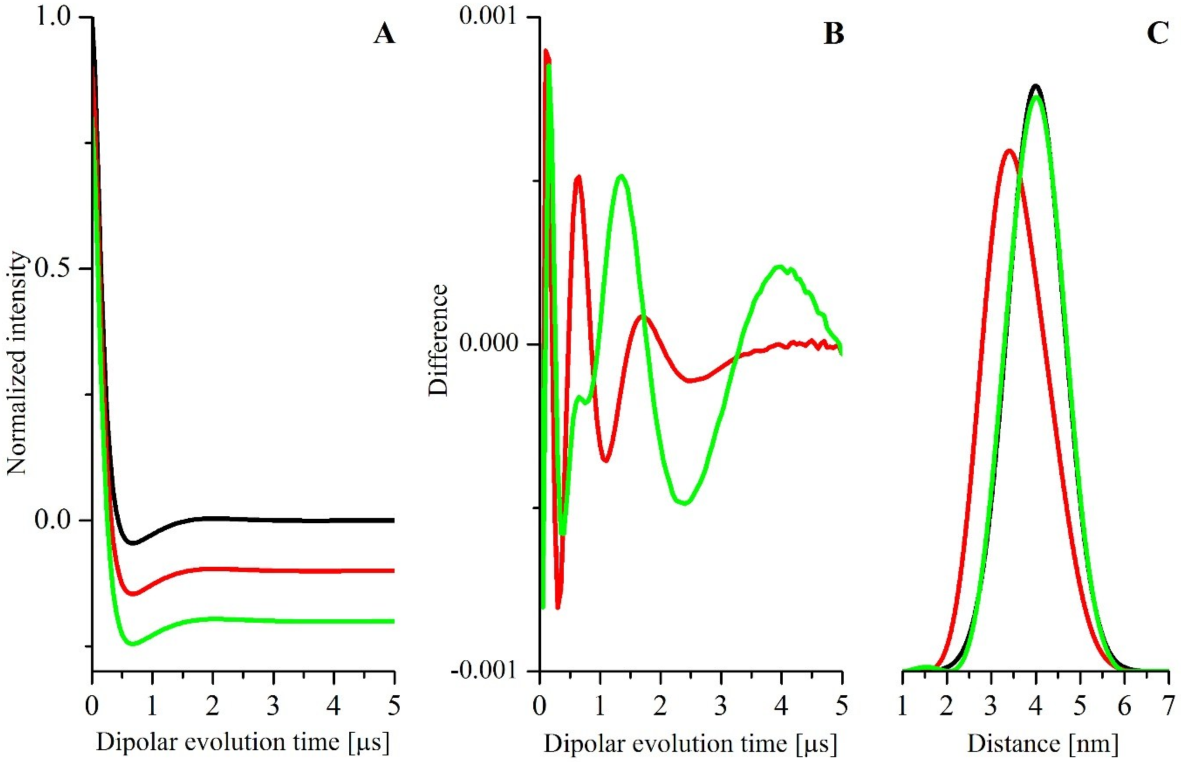

Figure S34. **(A)** Generated RIDME time trace (black) with back-calculated time traces, based on Tikhonov regularization analysis with the conventional kernel function (red) and the modified kernel function (equation 4 in the main text) (green). The time traces were vertically shifted for better visual comparison. Regularization parameter was 100. In-house written code was used for performing Tikhonov regularization. **(B)** Differences between calculated RIDME time trace and back-calculations, based on Tikhonov analysis with the conventional kernel (red) and the modified kernel function (equation 4) (green). **(C)** Distance distributions: input Gaussian distance distribution (black), distance distributions yielded by Tikhonov regularization with conventional kernel function (red) and kernel function (equation 4) (green).

13. Background functions in RIDME experiments

Background functions in the RIDME time traces were fitted by a stretched-exponential function: $y = A \cdot e^{-\left(\frac{t}{\tau}\right)^{\gamma}}$ with parameters given in Table S1.

Table S1. Parameters of the stretched-exponential functions for backgrounds in RIDME experiments

RIDME time trace	**A**	**τ [μs]**	**γ**
W-band, 20 μs mixing time, deuterated solvent	0.6903	3.8244	1.6782
W-band, 80 μs mixing time, deuterated solvent	0.4513	2.7676	1.6046
J-band, 30 μs mixing time, deuterated solvent	0.6280	2.6381	1.7725
W-band, 80 μs mixing, protonated solvent	0.4572	0.6116	1.8945
J-band, 25 μs mixing time, protonated solvent	0.5936	0.8386	1.9619

14. Assessment of ambiguity of background definition in RIDME and its influence on Tikhonov regularization analysis

The stretched exponential function is an adequate model for the background decay in RIDME experiment, but there is one source of ambiguity in its definition, the point in the time trace which is selected to be the starting point for the background fit. This is important since the initial part of the experimental time trace has a strong impact on the Tikhonov regularization analysis and poor background modelling can lead to distortions in distance distribution. Thus, in order to test how the initial point selected influenced the results of the Tikhonov regularization analysis, we incremented this point every 112 ns throughout the RIDME time traces and performed correspondingly the modified Tikhonov regularization analysis.

14.1 W-band RIDME with mixing time of 20 μs

The raw experimental RIDME time trace and the background functions, defined at multiple initial positions of the time trace, are shown in Figure S35 (left). The stretched exponential background functions were defined at 15 initial positions starting from 96 ns (position "start$_1$" in Figure S35) till 1664 ns (position "start$_{15}$") with a step of 112 ns. The correspondingly background-divided RIDME time traces are shown in Figure S35 (right). The figure shows that the background functions defined at initial points corresponding to 1552 ns and 1664 ns do not properly model the background decay. However, it is instructive to see, how such improperly modelling affects the Tikhonov regularization analysis.

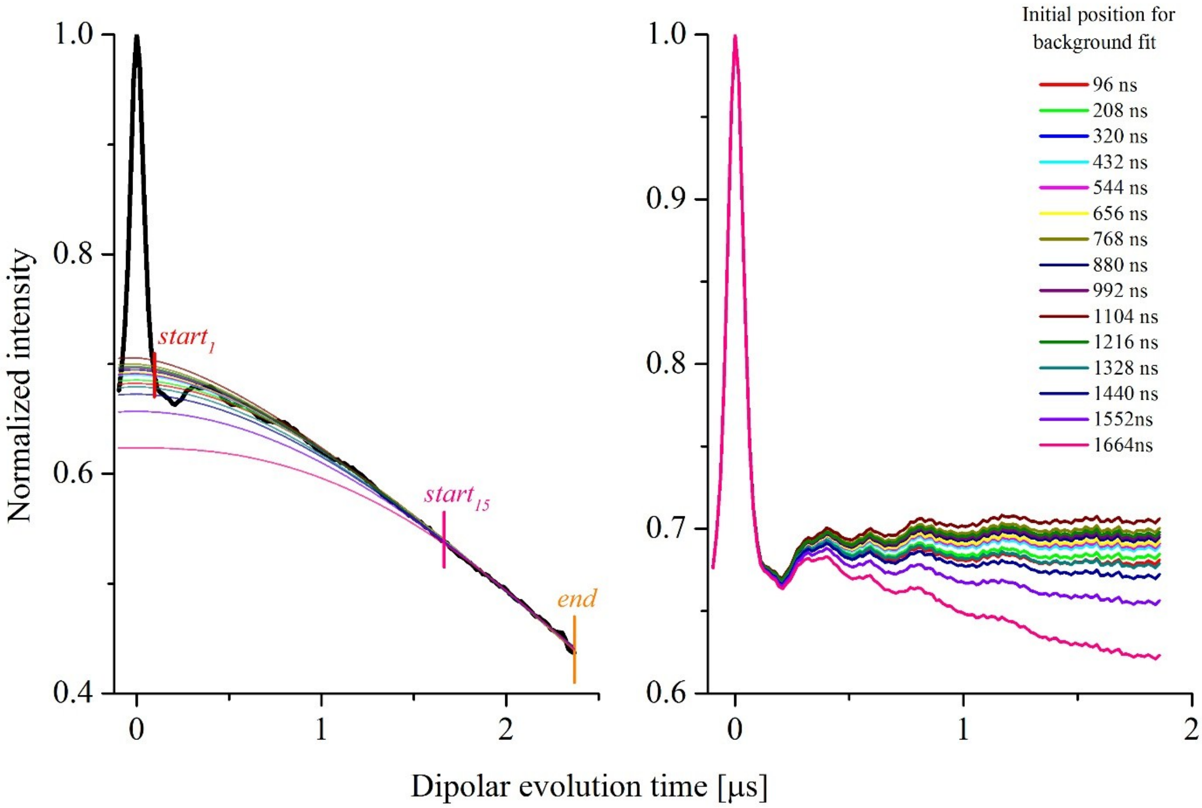

Figure S35. Left: Raw experimental RIDME time trace with 20 μs mixing time obtained on complex **1** in deuterated solvent (black) and background functions. Right: Background-divided RIDME time traces.

Results of Tikhonov regularization analysis, using kernel function (4), are shown in Figures S36 and S37.

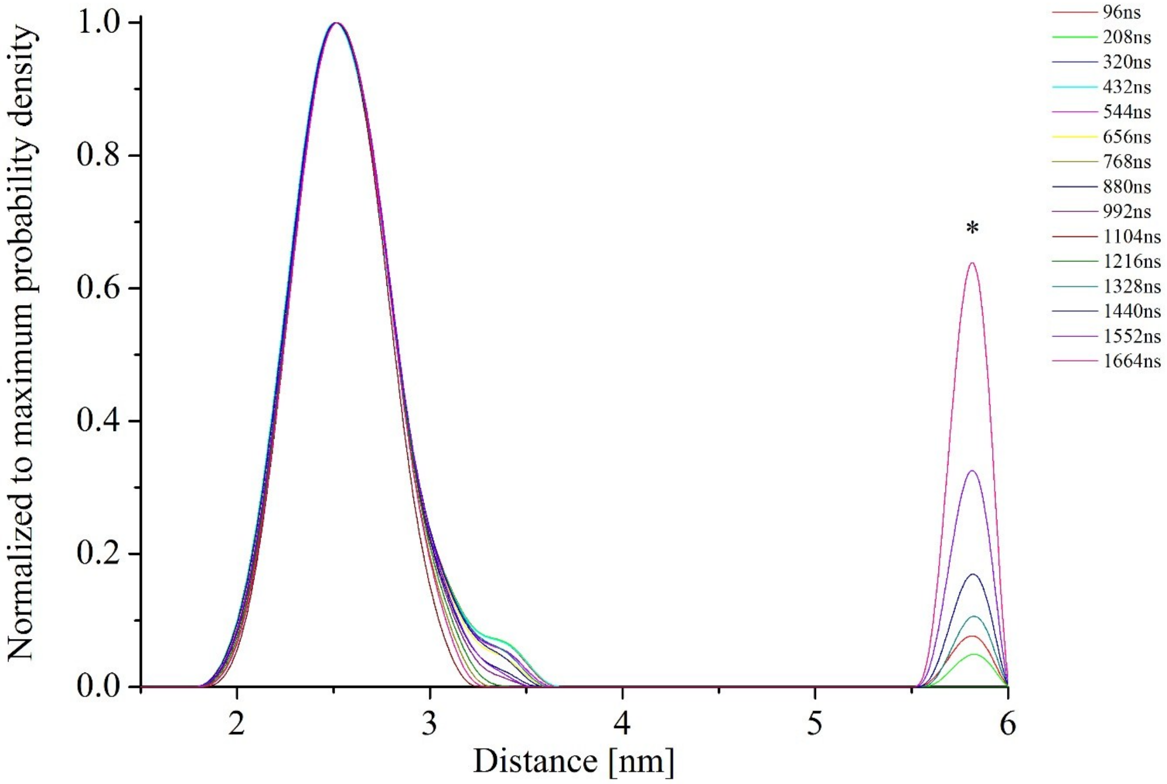

Figure S36. Distance distributions obtained by Tikhonov regularization analysis of the background-divided RIDME time traces (20 µs mixing time, deuterated solvent) shown in Figure S35. The distance distributions were normalized to the probability density of the most probable distance.

As can be seen from Figure S36, no significant effect on the main distance peak was observed, even when using 1552 ns and 1664 ns as initial points (Figure S35). However, additional distance peak at about 5.8 nm appeared, which was especially intense for the imperfectly defined background functions.

The background-divided RIDME time traces with correspondingly back-calculated time traces, based on Tikhonov regularization analysis with kernel function (4), are shown in Figure S37. For the background functions with defined initial points at 96 ns to 1440 ns, only insignificant changes of the dipolar modulation depths were observed (Figure S37). For the time traces corresponding to backgrounds, with defined initial points at 1552 ns and 1664 ns, deviation of modulation depths was stronger.

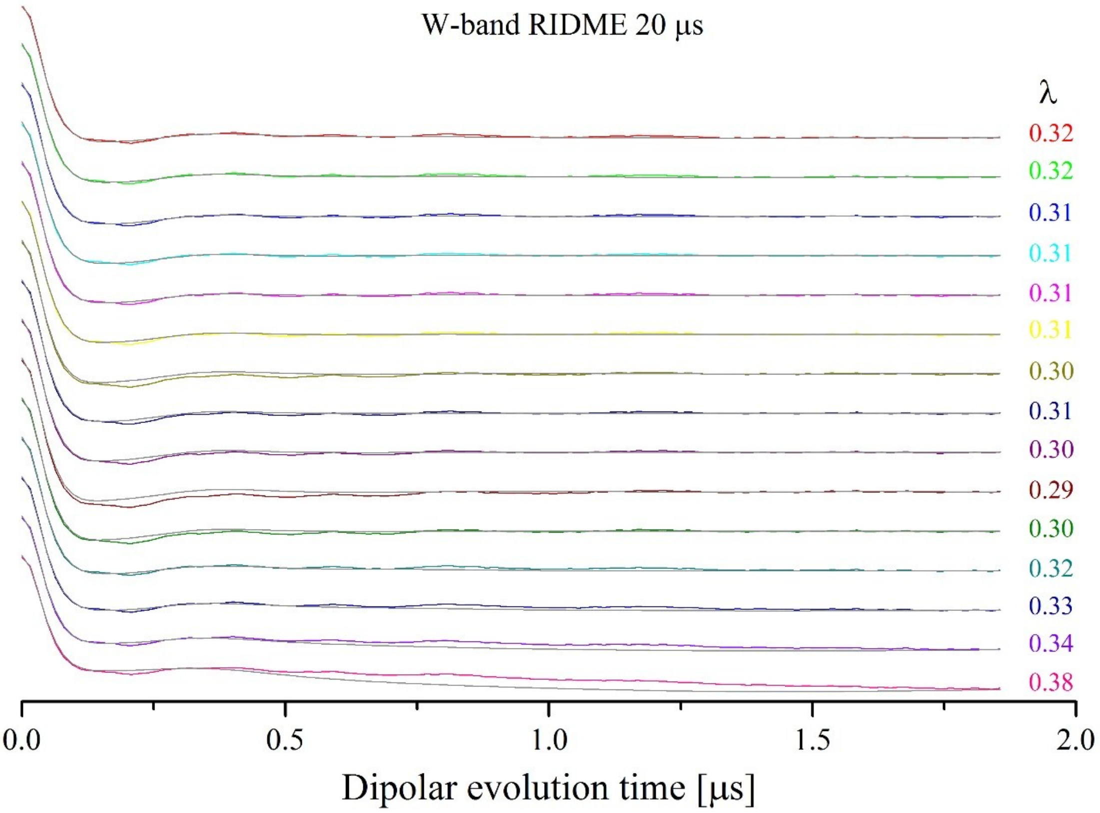

Figure S37. Background-divided RIDME time traces with 20 μs mixing time obtained on complex **1** in deuterated solvent (color-code is consistent with Figures S35 and S36) and back-calculations, based on Tikhonov regularization analysis (gray).

14.2 W-band RIDME with mixing time of 80 µs

The raw experimental time trace, corresponding background functions and background-divided RIDME time traces (80 µs mixing time) are shown in Figure S38.

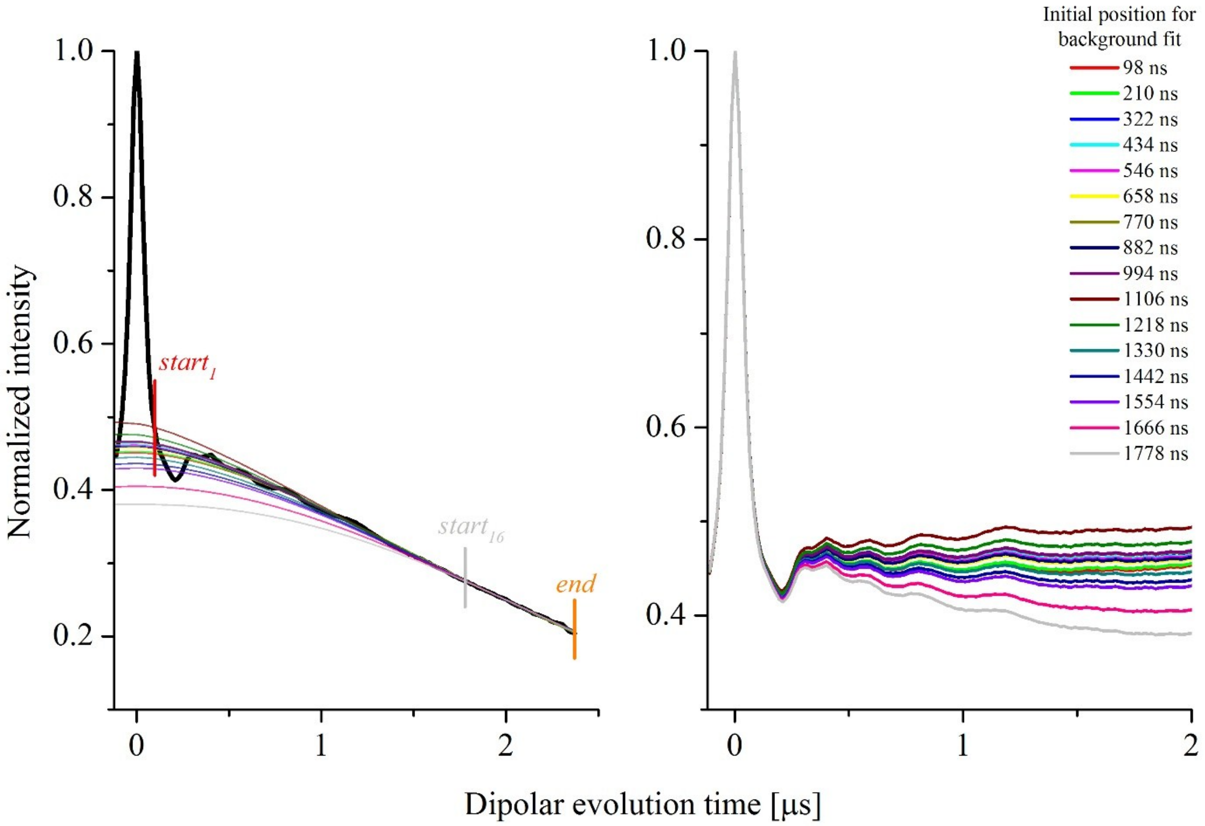

Figure S38. Left: Raw experimental RIDME time trace with 80 µs mixing time obtained on complex **1** in deuterated solvent (black) and background functions. Right: Background-divided RIDME time traces.

The corresponding distance distributions obtained by Tikhonov regularization analysis with kernel (5) and background-divided time traces overlaid with back-calculation are shown in Figures S39 and S40, correspondingly.

As with the W-band RIDME with 20 µs mixing time, we kept two imperfect background functions in order to study their influence on the Tikhonov regularization analysis. As can be seen in Figure S39, the main distance peak and the modulation depth did not strongly depend on the choice of the initial point used to model the background. However, increasingly poorer fits of background did lead to concomitant increase in the intensity of the distance peak at 5.8 nm and stronger deviation of the modulation depth.

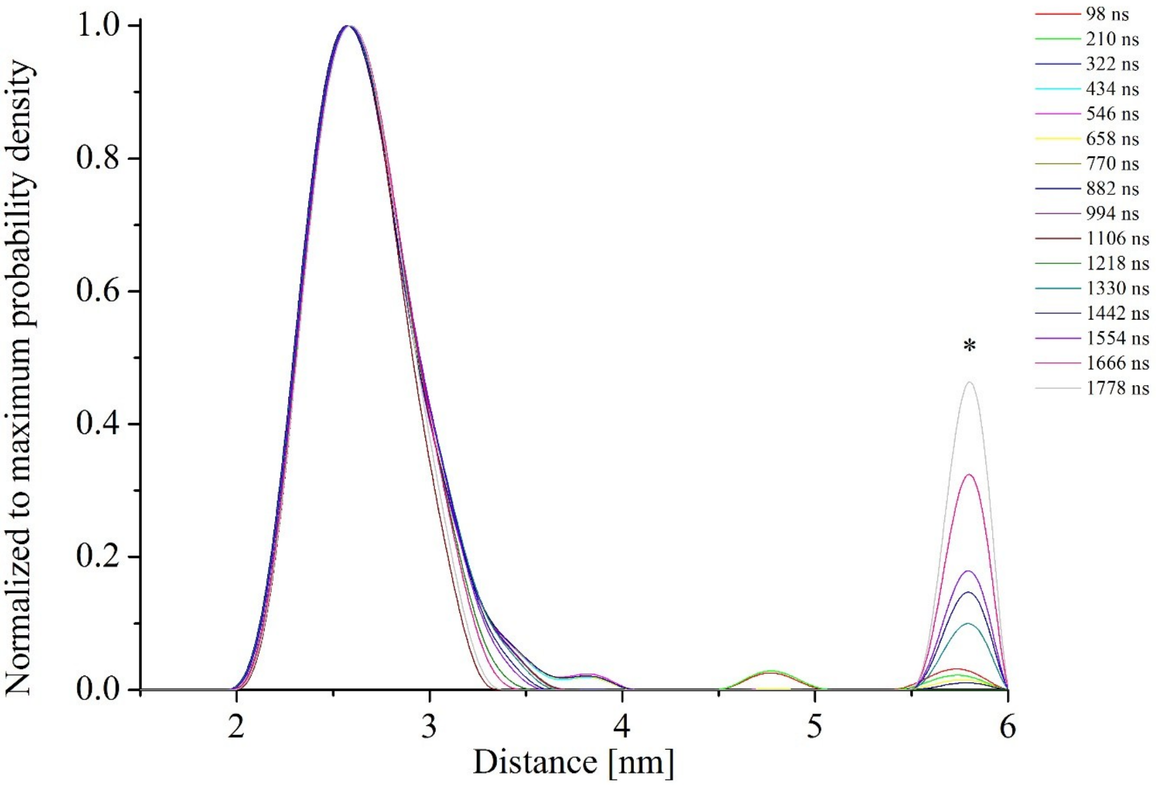

Figure S39. Distance distributions obtained by Tikhonov regularization analysis of the background-divided RIDME time traces (80 µs mixing time, deuterated solvent) shown in Figure S32. The distance distributions were normalized to the probability density of the most probable distance.

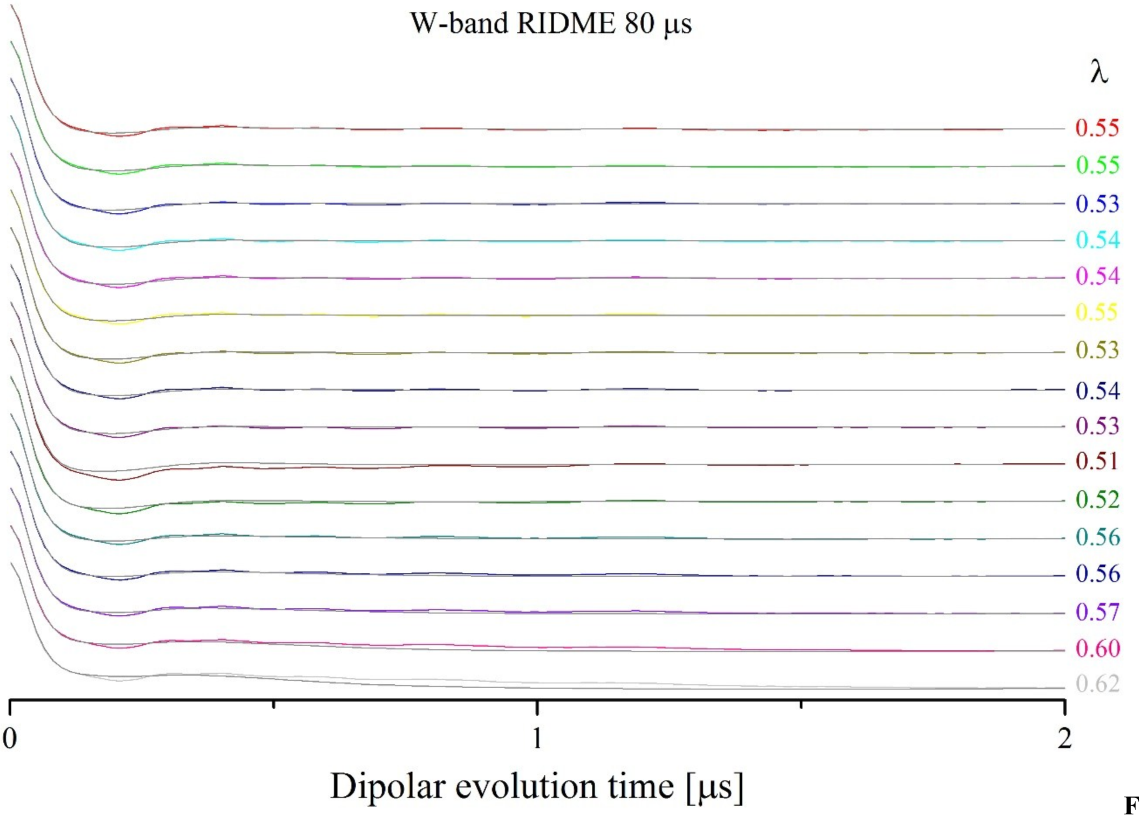

Figure S40. Background-divided RIDME time traces with 80 µs mixing time obtained on complex **1** in deuterated solvent (color-code is consistent with Figures S32 and S33) and back-calculations, based on Tikhonov regularization analysis (gray).

14.3 J-band RIDME with mixing time of 30 μs

The raw experimental J-band RIDME time trace, corresponding background functions and background-divided time traces are shown in Figure S41.

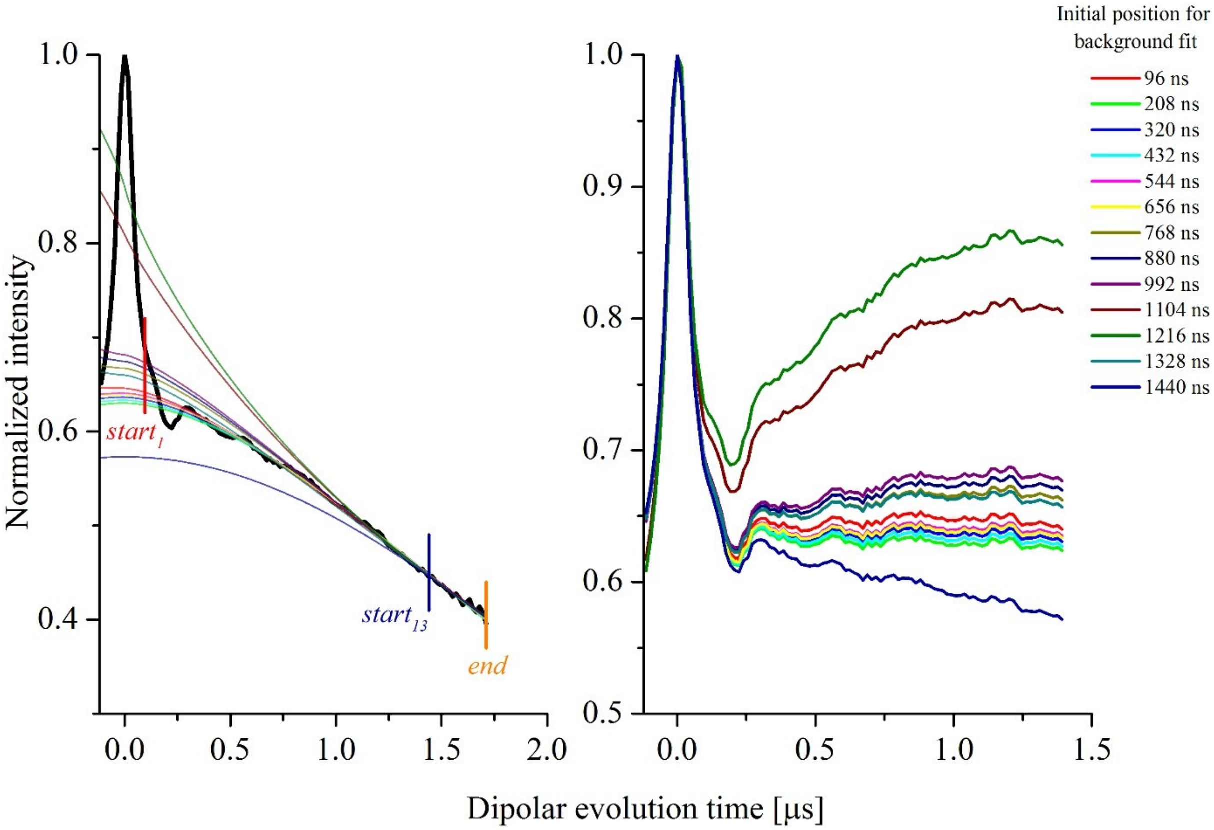

Figure S41. Left: Raw experimental J-band RIDME time trace with 30 μs mixing time obtained on complex **1** in deuterated solvent (black) and background functions. Right: Background-divided RIDME time traces.

As can be seen in Figure S41, two backgrounds (initial times of 1104 ns and 1216 ns) not only significantly deviated from the decay of the RIDME signal but qualitatively had different shapes. Therefore, such backgrounds and correspondingly background-divided time traces were excluded in further analysis.

The distance distributions obtained by Tikhonov regularization analysis with kernel (5) and background-divided time traces overlaid with back-calculation are shown in Figures S42 and S43, correspondingly.

As can be seen, differently defined background functions had greater impact on the shape of the main distance peak (Figure S42). We attribute such effect to the experimental imperfections of J-band RIDME time trace associated with the incomplete cancellation of the moving refocused stimulated and Hahn echoes (for more details see Section 8 and Figure S29).

In conclusion, the ambiguity of background definition of RIDME time traces on complex **1** in deuterated solvent had relatively small impact on Tikhonov regularization analysis and dipolar modulation depth.

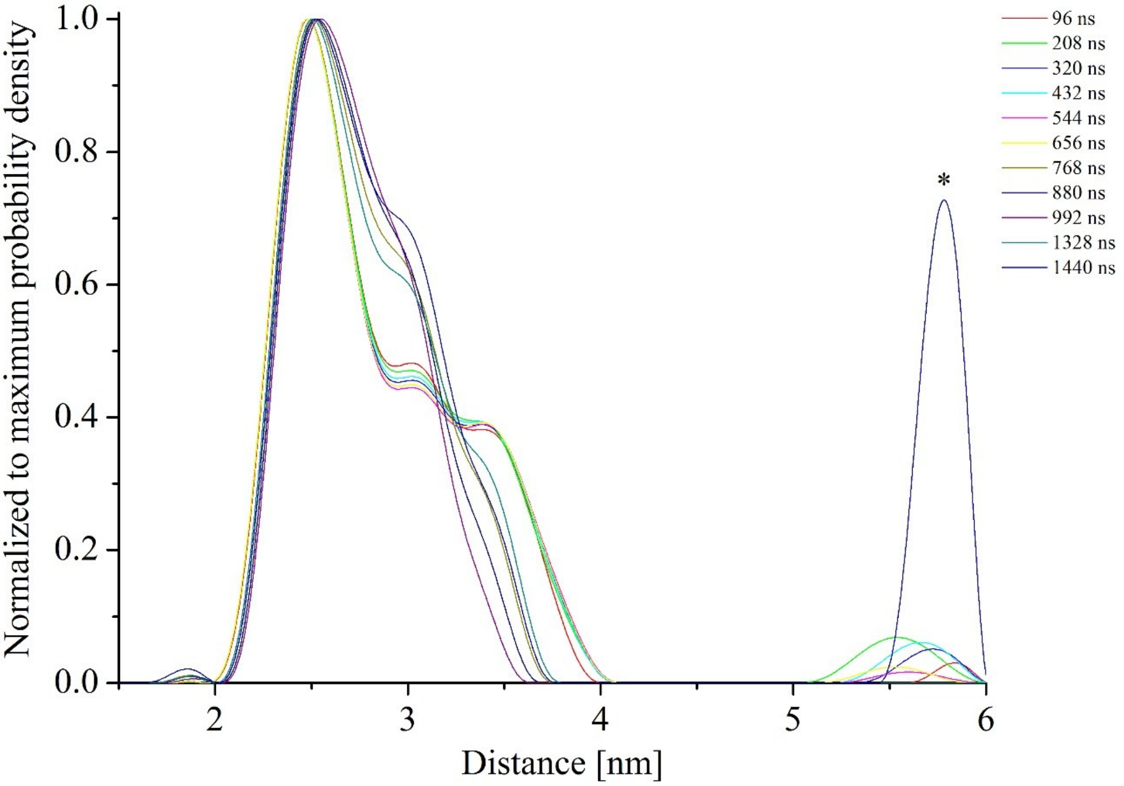

Figure S42. Distance distributions obtained by Tikhonov regularization analysis of the background-divided J-band RIDME time traces (30 µs mixing time, deuterated solvent) shown in Figure S35. The distance distributions were normalized to the probability density of the most probable distance.

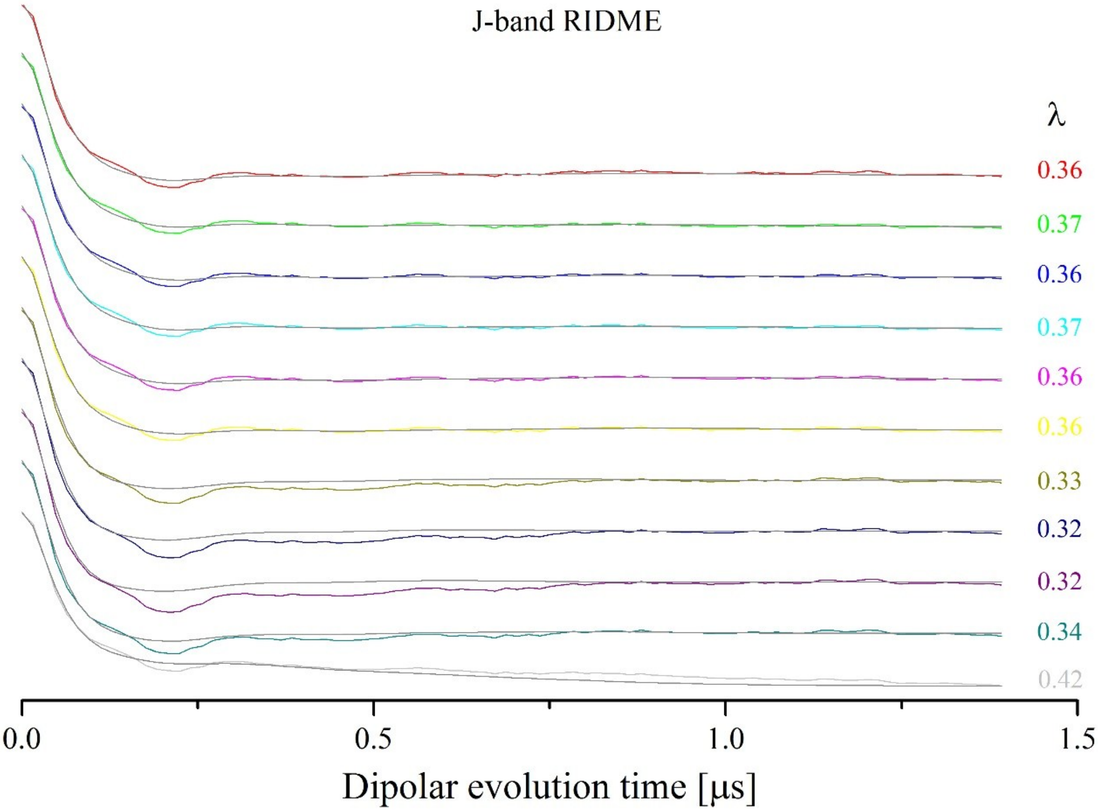

Figure S43. Background-divided J-band RIDME time traces obtained on complex **1** in deuterated solvent (color-code is consistent with Figures S35 and S36) and back-calculations, based on Tikhonov regularization analysis (gray).

15. Analysis of PELDOR and RIDME sensitivity

Relative sensitivity of PELDOR and RIDME measurements were estimated as signal-to-noise ratio (SNR) per square root of accumulation time:

$$
\begin{aligned}
&sensitivity \propto \frac{SNR}{\sqrt{t_{acc}}} = \frac{\lambda}{rms \cdot \sqrt{t_{acc}}}, \\
&rms = \sqrt{\frac{\sum_{j=1}^{N} \left(F_{j+1} - F_{j}\right)^{2}}{N}}
\end{aligned}
\qquad \text{(S3)}
$$

in which λ is the dipolar modulation depth of the corresponding measurement and *rms* is defined in the intervals with length, corresponding approximately to 10% of the whole length of the time trace, as defined in Figure S44. As the length of RDME time traces were longer than that of PELDOR, positions of the time intervals for RIDME were chosen consistently with PELDOR, as shown in this figure.

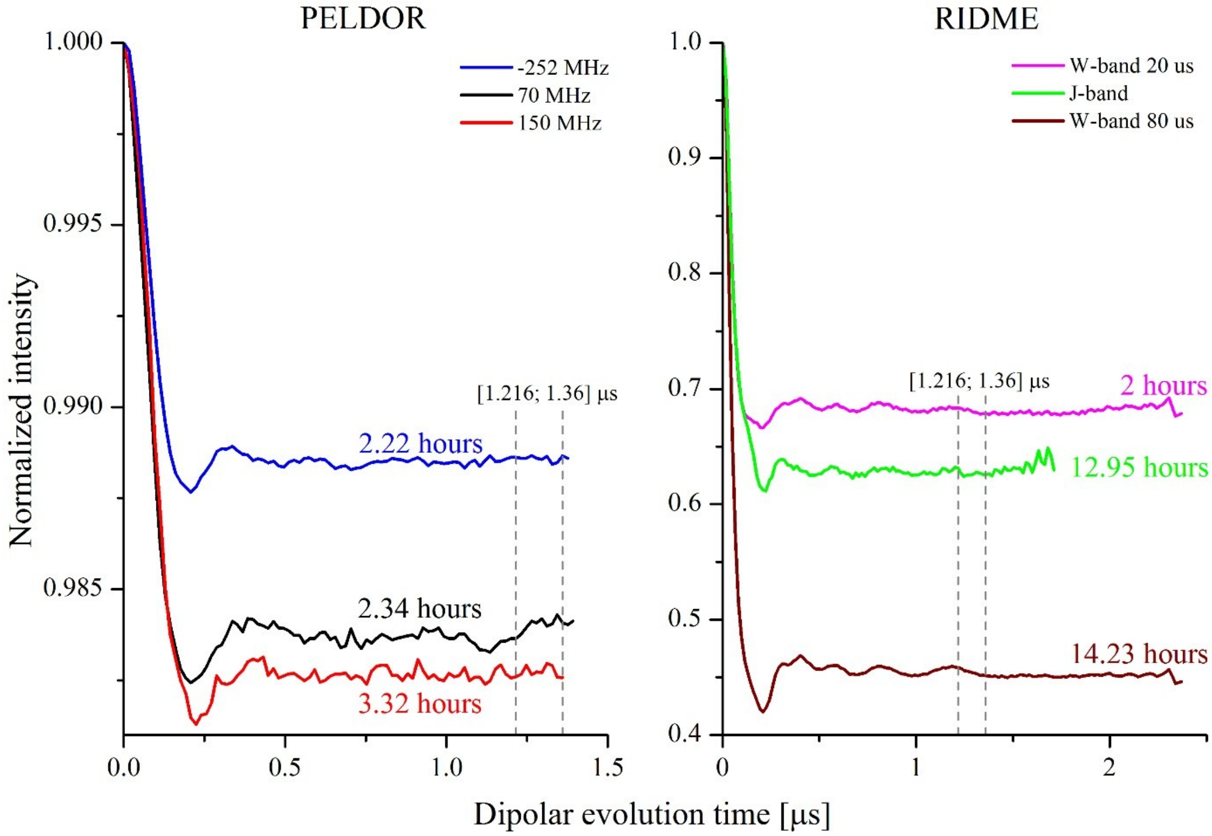

Figure S44. Background-divided PELDOR (left) and RIDME (right) time traces on compound **1** in deuterated solvent. Dashed vertical bars indicate time intervals, in which rms values are defined.

The values are summarized in Table 1 of the main text.

16. References

1. G. Jeschke, V. Chechik, P. Ionita, A. Godt, H. Zimmermann, J. Banham, C. Timmel, D. Hilger and H. Jung, *Appl. Magn. Reson.*, 2006, **30**, 473.
2. H. Y. V. Ching, P. Demay-Drouhard, H. C. Bertrand, C. Policar, L. C. Tabares and S. Un, *Phys. Chem. Chem. Phys.*, 2015, **17**, 23368.
3. L. V. Kulik, E. S. Salnikov and S. Dzuba, *Appl. Magn. Reson.*, 2005, **28**, 1.
4. S. Milikisyants, F. Scarpelli, M. G. Finiguerra, M. Ubbink and M. Huber, *J. Magn. Reson*. 2009, **201**, 48.